

1000001
1000002
1000003
73082

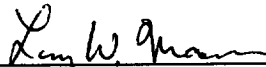
MCR-96-1303, Issue 02

Contract Number: NAS8-40633

Membrane Transport Phenomena (MTP)

Semi-Annual Technical Progress Report

May 1996 - November 1996



Principal Investigator, Program Manager:
Larry W. Mason

Prepared By:
Lockheed Martin Astronautics Company
Flight Systems Division
P.O. Box 179
Denver, CO 80201

Prepared For:
National Aeronautics and Space Administration
George C. Marshall Space Flight Center
Marshall Space Flight Center, AL 35812

LOCKHEED MARTIN

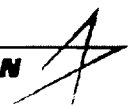


Table of Contents

MTP EXPERIMENT DEVELOPMENT	1
MEMBRANE TO FLUID OPTICAL CELL SEAL DEVELOPMENT	1
VOLUMETRIC FLOW SENSOR (VFS) DEVELOPEMENT	5
HYDROSTATIC PRESSURE EXPERIMENTS.....	6
MEMBRANE EVALUATION ACTIVITIES.....	8
MTA OSMOSIS EXPERIMENTS.....	10
Experimental Solutions	11
Experimental Data Acquisition.....	12
Solute on Top (+1g) Experimental Results.....	14
Solute on Bottom (-1g) Experimental Results	17
MTA FLUID MANIPULATION SYSTEMS (FMS) DEVELOPMENT.....	20
FMS SOFTWARE DEVELOPMENT.....	22
REFRACTOMETER IMAGE ANALYSIS SOFTWARE DEVELOPMENT.....	24
MTA REFRACTOMETER CALIBRATION.....	27
MTP ANALYTICAL MODEL DEVELOPMENT	33
DC-9 MICROGRAVITY EXPERIMENT DEVELOPMENT.....	37
Fluid Manipulation System (FMS) Experiment.....	37
Refractometer Verification Experiment (RVE).....	37
DC-9 Experiment Hardware Description	38
MICROSENSOR ARRAY DEVELOPMENT.....	42
MICROSENSOR ARRAY INTERFACE ELECTRONICS DEVELOPMENT.....	43

MTP EXPERIMENT DEVELOPMENT

The first generation instrument for the Membrane Transport Phenomena (MTP) experiment is complete, and is called the Membrane Transport Apparatus (MTA). The MTA is a prototype instrument that is designed to perform precision measurements on membrane mediated transport phenomena. Several subsystems of the instrument have been developed in parallel over the last six months. These subsystems are all interrelated, and the development activity was shared among the various systems as the instrument matured. The subsystems include: the membrane to Fluid Optical Cell (FOC) seal, data acquisition interfaces and software, and refractometer calibration and image processing software. Additionally, the MTA Fluid Manipulation System (FMS) has evolved to provide automatic control over filling and draining operations and the Volumetric Flow Sensors (VFS) have been upgraded. A series of experiments using the MTA have been conducted to calibrate the sensors, establish instrument sensitivities, characterize membranes, and measure osmosis. The subsystem development and experimental activities are detailed in following sections.

MEMBRANE TO FLUID OPTICAL CELL SEAL DEVELOPMENT

The development of the seal between the membrane and the Fluid Optical Cells (FOC) has been a high priority activity. This seal occurs at an interface in the instrument where three key functions must be realized: (1) physical membrane support, (2) fluid sealing, and (3) unobscured optical transmission.

This fluid cell seal provides physical support for the membrane. The membrane is secured around the perimeter, captivated by the fluid cell sealing surfaces and compressed between the two fluid cells. The fluids exert a hydrostatic force on the membrane that changes as the fluids move from one compartment to the other. The magnitude of the hydrostatic force (pressure head) is determined by the relative level of fluid within the two Volumetric Flow Sensors (VFS). As these levels change relative to each other, the force exerted on the membrane also changes, and the membrane physically moves. The movement of the membrane is restrained by the seal, and it can pull free from the seal if enough hydrostatic pressure is applied.

Several different materials were tested in the development of this sealing interface, and a variety of assemblies used to support the membrane. Figure 1 shows how the seal developed, and some of the assemblies that were tried in an attempt to create a leak free membrane to fluid cell seal.

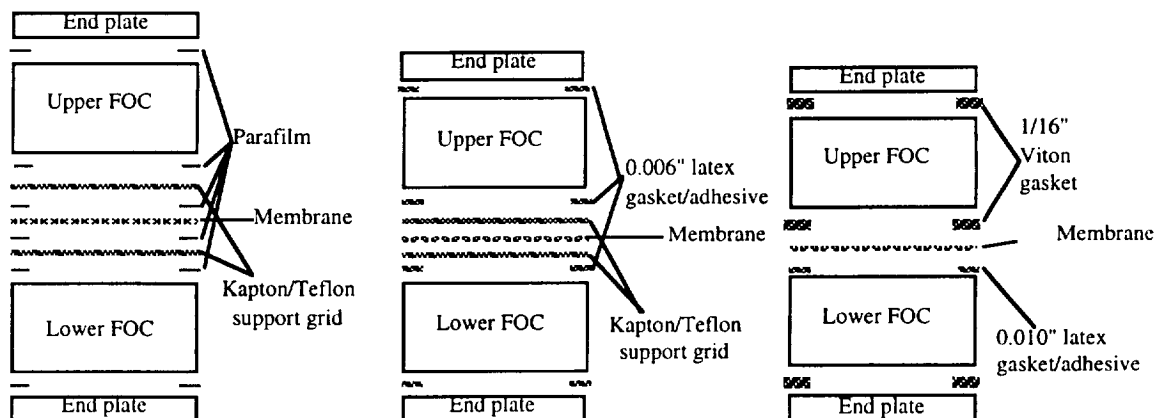


Figure 1 Membrane Support Assemblies That Failed

Parafilm, a waxy material that is commonly used in laboratories to seal glassware, was initially used to make sealing gaskets for the MTA. This proved not to be effective, either alone or in combination with membrane support grids. In another attempt, a sandwich assembly was created using alternating layers of Parafilm and Kapton with the membrane in the middle. This configuration also proved not to be functional in terms of fluid leaks.

Latex rubber sheet material was used to fabricate gaskets of various thickness for the membrane to fluid cell seal. Initially, a 0.006" thick latex gasket was fabricated in the appropriate shape and bonded to fluid cell sealing surfaces using double sided (3M) waterproof adhesive tape. This approach appeared to be promising because the latex gasket was bonded firmly to the glass FOC sealing surface, allowing the membrane to be positioned independent from the sealing gaskets. However, the latex material was too thin to provide an adequate seal around the membrane, and the "waterproof" adhesive proved to be water soluble when in constant contact with aqueous solutions. In addition, it was difficult to apply the adhesive to the gasket material evenly, and correctly position the gasket on the fluid cell sealing surface. The latex rubber gaskets were also used without adhesive with limited success. Figure 2 shows an example of this sealing configuration, where the disassembled MTA fluid cells are shown with a latex gasket seal positioned over a membrane.

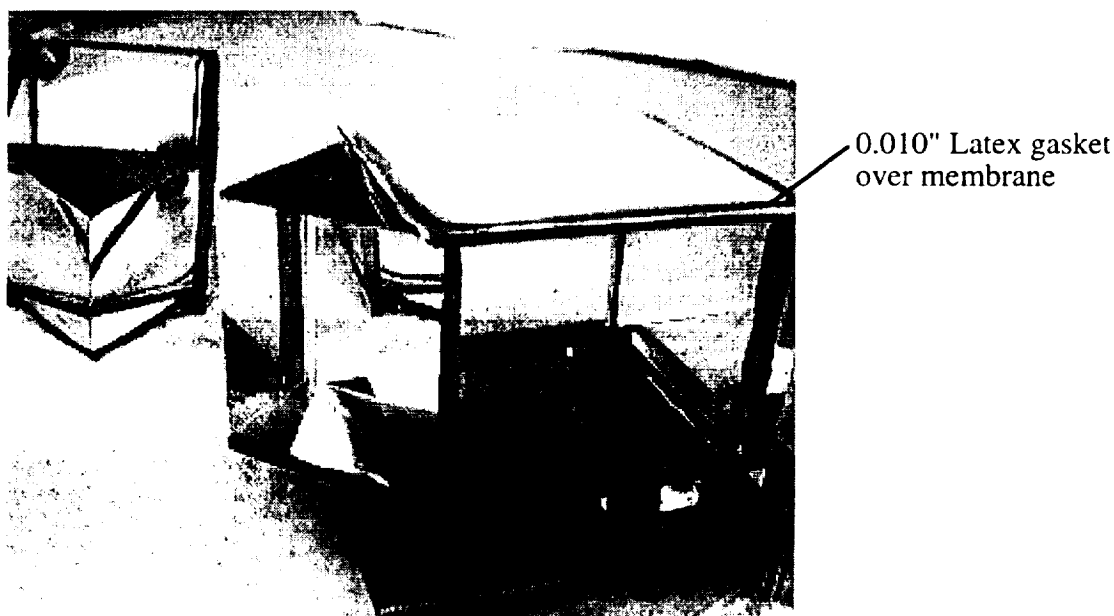


Figure 2 MTA Fluid Cells With Membrane and Latex Gaskets

Thicker latex material (0.010") was also tried with limited success. Successful sealing configurations were attained intermittently. Sometimes the compressive sealing force required to effect the seal between the optical cells was too high, and resulted in cracked epoxy in the fluid cell corners. The epoxy is used to hold and seal the glass and plastic walls of the FOC's together. Each time cracking occurred, the FOC's had to be rebuilt and the glass and plastic sealing surfaces repolished. Between the FOC rebuild cycles, there were some times where no leaks were found and experimental data was acquired. The refractometer calibration and membrane evaluation experiments were performed using these leak free configurations, as described in other sections of this report.

It is critical that no leaks are present in either of the fluid cells (upper or lower) during osmosis experiments. The flow that results from a leak is detected by the Volumetric Flow Sensors, and can be incorrectly interpreted as solvent flow through the membrane. There are two types of leaks that can occur at the membrane to fluid cell interface: (1) leaks from either fluid cell to the outside, (2) a leak from one fluid cell to the other. Each of these leak types has occurred during the instrument development. Figure 3 shows the data acquired from a leaky seal configuration with the SEPA CF (5000 MWCO) membrane. Each tick mark on the x-axis represents one hour. Initially there was a single leak present between the two fluid cells and the fluid levels come together as the hydrostatic pressure equalizes between the two fluid cells. After about two hours, a second leak developed in the lower fluid cell, and both fluid cells show a decrease in fluid volume with time. The leak was probably located in the lower fluid cell because the lower cell fluid volume decreases faster than the upper cell. This leak was located in the seal between the two prisms. Many other experiments also showed leaks in various locations along the seal.

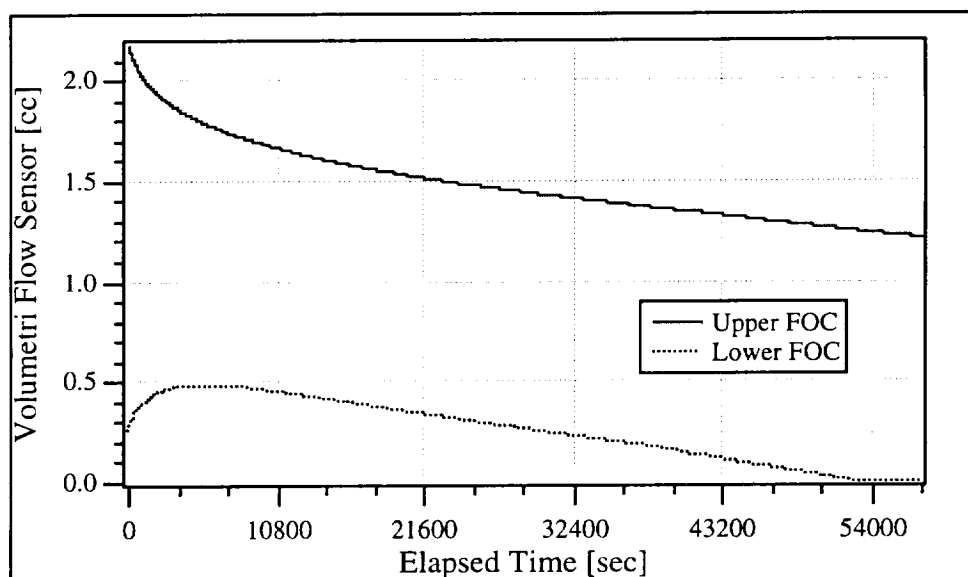


Figure 3 Experimental Data Showing Fluid Leak in Upper Fluid Optical Cell

It is difficult to distinguish between a leak between the two fluid cells and solvent flow through the membrane in response to hydrostatic pressure. This is especially true if the leak is small, and the membrane characteristics are not known from prior experience.

The third facet of the membrane to fluid cell seal is the interface to the optical refractometer. The physical dimension of the seal interferes directly with the refractometer beam so the thickness of the fluid cell material must be minimized. The refraction beam is used to visualize the solution refractive index profile and boundary layer formation dynamics. It is desirable for the refraction beam to pass as close as possible to the membrane to allow observation of this critical fluid volume. This requirement is in direct conflict with the need to effectively seal the fluid cells: the thinner the sealing material, the less effective the seal.

A membrane to fluid cell sealing configuration was eventually developed that resulted in a leak free configuration. This design represented a compromise between the two opposed requirements for sealing and visualization. It provided a leak free seal between the fluid cells and the membrane, and minimized obscuration of the refractometer beam in the area where the fluid boundary layer forms. The seal was comprised of two gaskets with the membrane held in between, the upper gasket made from 1/32" Viton, and the lower gasket made from 0.010" latex rubber. The membrane was captivated between the two gaskets,

creating a seal between the fluid cells and the membrane. The thicker Viton gasket provided the sealing compliance for the membrane to fluid cell interface, and the lower gasket was very thin to allow visualization of the refractive index profile on the lower side of the membrane. The Viton gasket compressed to about 1mm thickness when in the MTA, obscuring the refractometer beam only on the upper side of the membrane. The latex rubber gasket obscured less than 0.2 mm of the refractometer beam, allowing visualization of the lower side of the membrane and boundary layer formation dynamics. The boundary layer forms only on the lower side of the membrane, and the thicker Viton gasket did not interfere with the refractometer optics on the lower side.

This membrane seal configuration was functional, but proved difficult to maintain. When the membrane and sealing components were assembled, the membrane had to be trimmed and installed through trial and error until no leaks were detected. The physical size of the membrane was critical, it had to cover a large enough portion of the fluid cell sealing surface to be compressed by the fluid cells, and leave enough of the gasket material exposed to the edges to create a seal. Additionally, the relative positions of the two gaskets, the membrane, and the optical cell sealing surfaces all had to be aligned exactly to effect the seal when the entire assembly was installed within the support frame. If any of these components was out of position by even 0.4 mm, a leak resulted. Further, a large compressive sealing force was required to insure that the sealing gaskets contacted each other around the membrane periphery. On occasion, this compressive force proved to be destructive to the epoxy seals that hold the FOC optical components together. When the epoxy became detached or cracked, the prism and side windows had to be completely disassembled, re-epoxied, and the sealing surfaces re-polished.

The Viton and latex sealing configuration of Figure 3 showed leak-free operation for about 3 weeks, and several osmosis, calibration, and membrane evaluation experiments were performed during this time. One experiment was performed using a high viscosity solute (Polyethylene Glycol or PEG). During the pumping operations to fill and drain the fluid cells, excessive hydrostatic force was exerted on the membrane causing it come loose from the seal, resulting in what has been termed a "blown membrane". Figure 4 shows a picture of the blown membrane in the MTA. The leak between the fluid cells occurred at the membrane crease, located at the center of the FOC prisms.

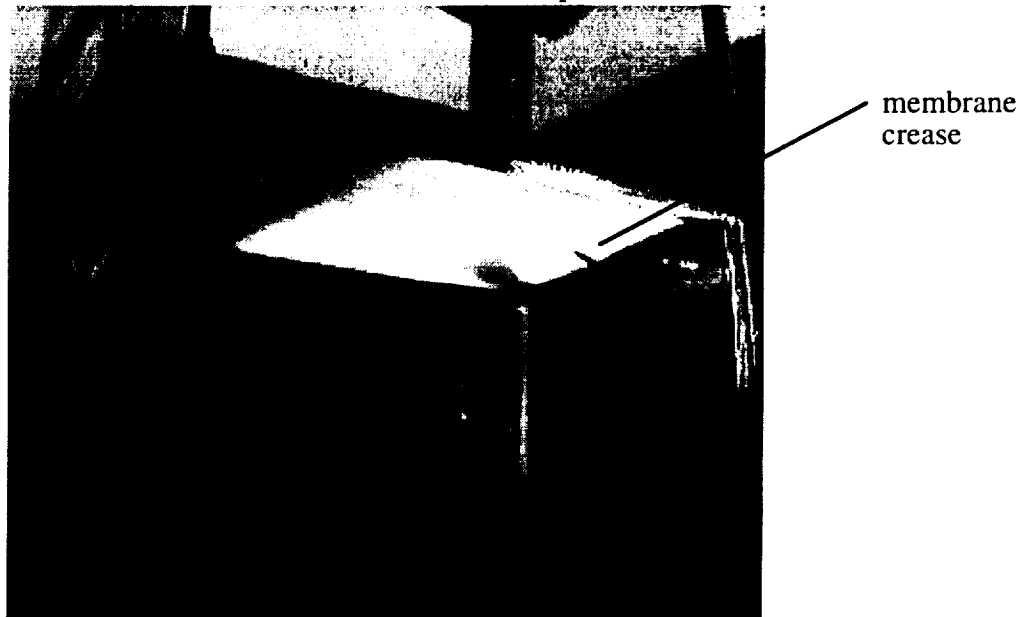


Figure 4 Blown Membrane Causing a Leak Between the Fluid Optical Cells

The high pressure across the membrane was caused by a combination of the high viscosity solute, and malfunctioning valves. The valve malfunction is described in the Fluid Manipulation System section of this report. The blown membrane required that the MTA be disassembled to replace the membrane. During this activity it was seen that the epoxy had loosened in a corner of the lower FOC, at it was beginning to leak. This was presumably caused by the high compressive force required to effect the seal. The fluid cell assembly had to be completely rebuilt and sealing surfaces re-polished. After rebuilding, the leak-free configuration was not attainable using these same sealing materials.

The next step in the MTA seal development was to use thicker gaskets to decrease the positioning accuracy requirements and insure that a seal was attained around the entire perimeter of the membrane. Two 1/32" thickness Viton gaskets were used to captivate the membrane and create the seal. This configuration has not leaked to date. The thicker gaskets obscure the refractometer beam to a distance of 1 mm on each side of the membrane surface. Figure 5 shows a schematic diagram of this leak-free membrane sealing assembly configuration.

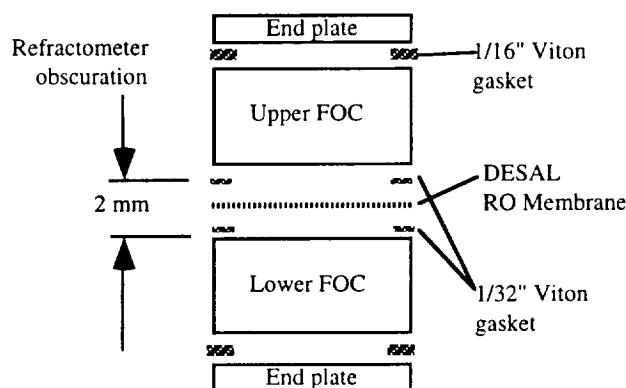


Figure 5 Leak-Free Configuration of the MTA Membrane Sealing Assembly

This membrane seal configuration has become the nominal baseline for all of the MTA experiments. It represents a compromise between the ability to effect a fluid seal using the current fluid cell design, and the refractometer visualization of the fluid boundary layer adjacent to the membrane. Further development of the membrane seal is not practical at this time, considering the MTP program schedule and upcoming Science Concept Review. Development of a thinner membrane seal assembly should be possible using optical components of smaller dimensions. Components of smaller dimensions should also allow visualization of the boundary layer closer to the membrane surface than the current design allows, while maintaining the fluid seal integrity. Additional fluid cell definition activities are planned during the upcoming DC-9 microgravity flight experiments.

VOLUMETRIC FLOW SENSOR (VFS) DEVELOPEMENT

The electrical interface circuit for the Volumetric Flow Sensors was upgraded to minimize long term drift and ambient temperature effects. Prior to this upgrade, differentiation of the VFS signal with respect to time to calculate flow rates showed an unacceptable amount of noise. The noise was traced to fluctuations in the voltage supply and long term drifts that correlated with ambient temperature changes. The VFS circuit upgrade involved the addition of an on-board voltage regulator to minimize source voltage fluctuations associated with the circuit DC power supply. The additional electronic components were added to the existing sensor interface circuit.

The data acquisition software for the VFS system was also upgraded. The upgraded software allows specification of the acquisition speed and resolution of the VFS data. Course resolution data can now be acquired at high speed for fluid manipulation operations. The increased acquisition speed is useful during the closed loop pumping operations to minimize the time lag associated with data acquisition. Slower, high resolution data is acquired during the osmotic and hydrostatic flow experiments. The sensor noise problem was further reduced by acquiring the sensor reading over a one second interval, and averaging the value. The time averaging increased the signal to noise ratio of the data, and dramatically lowered the scatter in the differentiated VFS data.

A calibration protocol was developed for the VFS. This protocol involves first calibrating the peristaltic pumps using a mass balance to measure pumped volumes. The calibrated volumes are then pumped into the VFS and the sensor outputs recorded. The solvent mass contained within the VFS can then be correlated to the sensor output signal using a regression analysis. The sensors were shown to be linear devices. Two coefficients are defined that can be used to convert the voltage output to contained VFS solvent mass. Both VFS were re-calibrated with DI water for use in the osmosis and hydrostatic experiments. The calibration software for both the peristaltic pumps and the VFS were developed in conjunction with the MTA Fluid Manipulation System (FMS), described in another section of this report.

HYDROSTATIC PRESSURE EXPERIMENTS

During the membrane to fluid cell seal development, membranes of different types were tested in the MTA for sealing, deformation, and hydrostatic flow characteristics. These experiments were conducted as the development of the MTA seal allowed, and were used to characterize the seal assemblies and membranes. An experimental protocol and data analysis software were designed to evaluate the hydrostatic flow characteristics of the various candidate membranes. The leak data shown previously in Figure 3 was acquired using this procedure. Figure 6 shows data from an example hydrostatic experiment, where the upper trace represents the level of water in the lower fluid cell, and the lower trace represents the level of water in the upper fluid cell as a function of time.

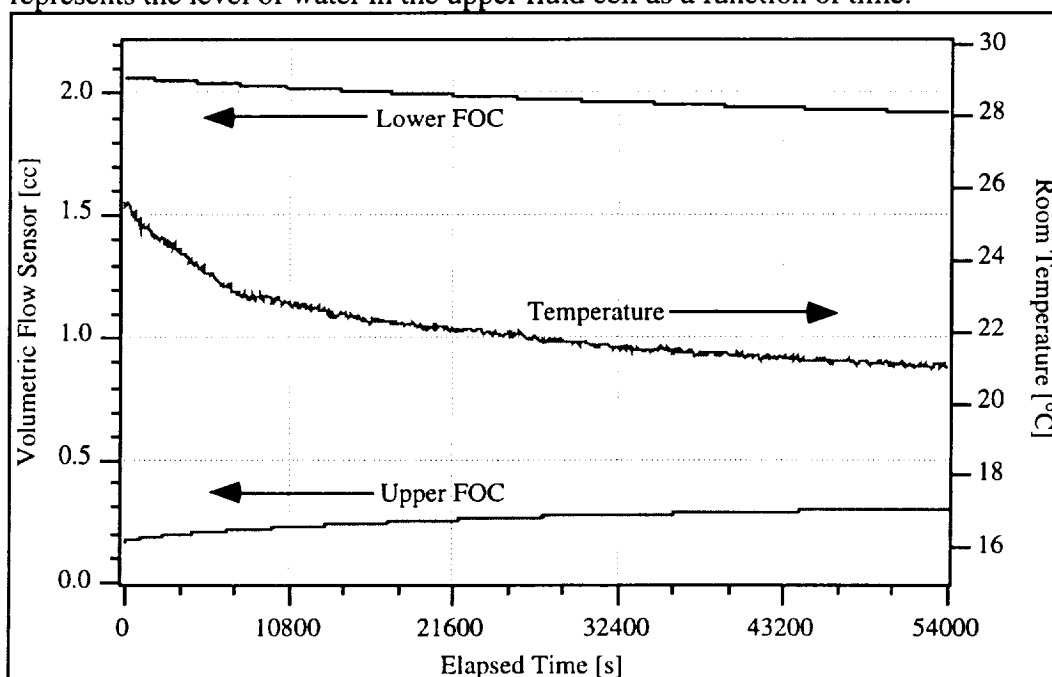


Figure 6 Data from Hydrostatic Test of DESAL RO Membrane

The hydrostatic experiments consist of first establishing a leak-free membrane sealing configuration, then applying a measured hydrostatic pressure across the membrane, and collecting kinetic data for solvent flow through the membrane. The hydrostatic driving force in the MTA is defined by the difference in fluid level between the two fluid cells, each filled to a different level with deionized water. The two Volumetric Flow Sensors are secured at the same height relative to the fluid cells, but are filled with fluid to different levels. When one VFS is full and the other almost empty, a maximum of about 4" of pressure head is present across the membrane. The displacement of each membrane tested under the influence of this pressure was observed and noted, and data collected for solvent flow using the VFS. As the hydrostatic pressure caused water to flow through the membrane, the level in each of the volumetric flow sensors changed, and was recorded as a function of time. The levels in the two Volumetric Flow Sensors come together as the hydrostatic pressure across the membrane equalizes.

Data from these tests was analyzed to measure the trans-membrane flow rate as a function of hydrostatic pressure. The flow rate was determined as the derivative of the Volumetric Flow Sensor data with respect to time (dV/dt), in units of cc/sec. Figure 7 shows the data processed in this way for the upper FOC. The flow rate is positive because water flowed through the membrane into the upper fluid cell, and it gained volume over the course of the experiment. After the initial (0.5 hour) transient, the flow rate became relatively constant.

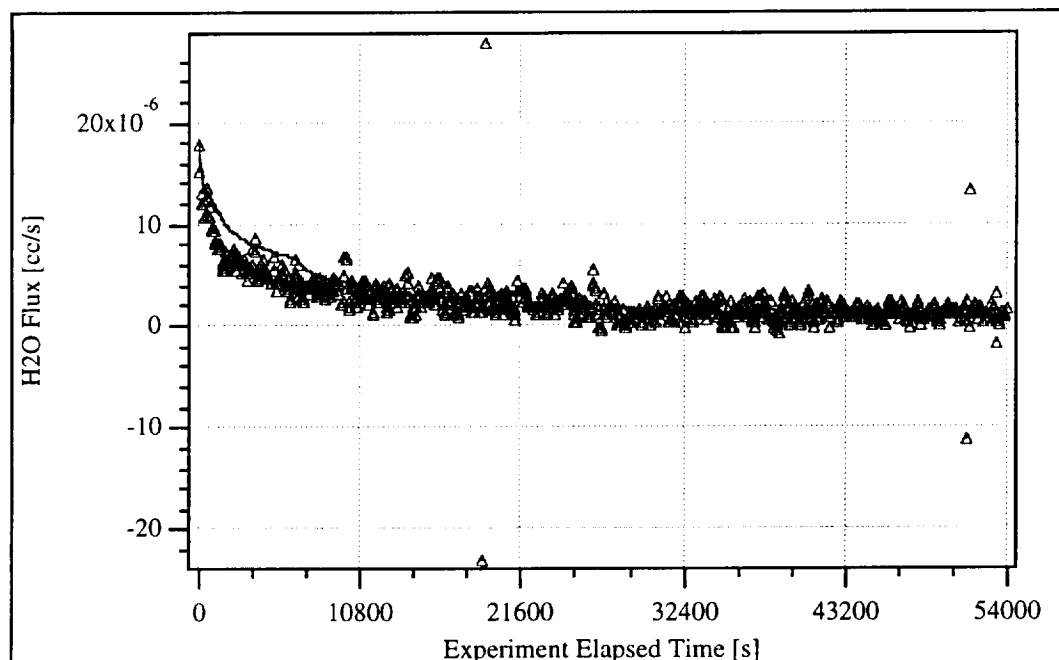


Figure 7 Data From a DESAL RO Membrane Hydrostatic Test, Differentiated to Show Solvent Flux Through the Membrane from the Upper FOC

The DESAL membrane used in this experiment is designed for Reverse Osmosis (water purification) applications, where a very large hydrostatic pressure (hundreds to thousands of psi) is used to drive water molecules through the membrane in a direction opposite to the chemical potential gradient, thus Reverse Osmosis. The hydrostatic pressure used in these MTA experiments is very small in comparison, and it is not surprising that the water flow rate was nearly constant, and independent of the driving hydrostatic pressure.

MEMBRANE EVALUATION ACTIVITIES

Several membranes were tested for hydrostatic flow characteristics, as the membrane seal and refractometer calibration activities allowed. The membranes were evaluated with respect to physical displacement in the MTA and solvent flow from the applied the hydrostatic pressure. Table 1 lists the membranes that were subjected to these hydrostatic tests and the results in terms of MTA applicability.

Table 1 Membranes Tested and MTA Applicability

Membrane Mfr	ID	Displacement From Edge	Hydrostatic Flow Characteristics	MTA Applicability
Osmonics	SEPA CF SS-10 0.001 μm pore	6 mm	variable: 20-200 nl/s	-excessive pillowing
Whatman	5000 MWCO 0.003 μm pore	~ 2mm	variable: 1-20 nl/s	-moderate pillowing - hydrostatic flow polarization - pore size too large
Whatman	Cellulose Acetate 0.22 μm pore	~ 4 mm	100 $\mu\text{l/s}$	-excessive pillowing -pore size too large
DESAL	RO-11 thin film 0.0004 μm pore	< 2mm	constant: ~1 nl/s	-minimal pillowing -osmotic flow polarization

The membrane displacement is a measure of the physical “pillowing” in response to the applied hydrostatic pressure, and was measured as the position of the center of the membrane relative to the membrane edge (sealed between the upper and lower FOC’s). The membrane pillowing effect alters the internal geometry of the Fluid Optical Cell. Depending on the magnitude of the pillowing, the fluid volume next to the membrane no longer has a constant cross sectional area. As a result, the refractive index profile is seen to change when translation motion is applied to the MTA relative to the laser, scanning the refraction beam across the membrane, similar to an edge effect in the fluid. The pillowing effect masks the one dimensional geometry within the cell, and a one dimensional transport model no longer describes the system. Smaller displacement is also preferable to minimize membrane interference and obscuration of the refractometer light beam.

The Osmonics membrane showed extreme displacement in response to the hydrostatic pressure. This problem worsened with time, as the membrane seemed to become more compliant and swell the longer it was exposed to water. Use of this membrane would require additional support structures adjacent to the membrane to maintain a planar configuration during MTA experiments. The support grids would interfere with the fluid flow patterns and the one dimensional geometry of the MTA. The membrane pore size (~0.001 μm) is small enough to accommodate all but the smallest of the colligative solutes planned for the MTA experiments, but the displacement problem is too extreme for this membrane to be suitable for the MTA.

The changing solute levels exert a changing hydrostatic pressure across the membrane. When the levels eventually cross, the hydrostatic pressure is zero and the flow rate would approach zero in a hydrostatic experiment. In an osmosis experiment, the chemical potential continues to drive water through the membrane. In some membranes, physical movement occurs until the membrane is completely pillowed in the opposite direction as the two fluid levels cross. This physical movement alters the fluid level in both the FOC’s, and is recorded along with the osmosis data as abrupt transient changes that show a decrease in one FOC that is correlated with an increase in the other. The nature and

abruptness of the movement is associated with how stiff the membrane material is, and how rapidly the fluid levels are changing. Figure 8 shows an example of the membrane movement, and the effects as recorded in the VFS data for the 5000 MWCO membrane. Excessive pillowing and membrane movement are unacceptable for the MTA application.

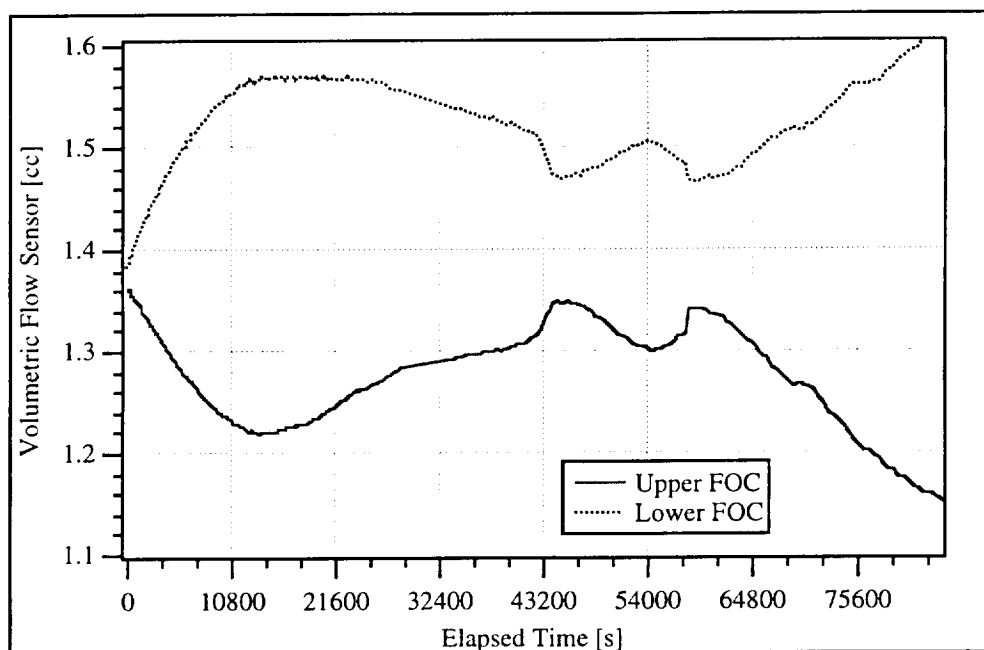


Figure 8 Membrane Movement Effects Caused by the Changing Hydrostatic Pressure Exerted Across the 5000 MWCO Membrane

The 5000 Molecular Weight Cut Off (MWCO) membrane also showed a hydrostatic flow polarization effect. The kinetics of hydrostatic water flow were different, depending on which direction the solvent was flowing through the membrane. This type of membrane is generally used for ultrafiltration applications (*i.e.*, protein purification) where the flow characteristics are not a major concern. The 30 angstrom pore size is too large to allow osmosis to occur with some of the lower molecular weight solutes planned for the MTA experiments. These factors all indicate that this membrane is not suitable for the MTA application. Similar physical characteristics were found with the 0.22 μm pore Cellulose Acetate membrane.

The DESAL Reverse Osmosis (RO) membrane was found to be superior to the all others tested, for the MTA application. It is comprised of a thin film (polyamide) membrane that is supported on a polyester base, and normally used for brackish water desalination and reactive silica removal in aqueous process streams. The stiff polyester support material minimizes the hydrostatic displacement (pillowing). The 4 angstrom pore size in the thin film membrane is compatible with the full range of solute molecular weights planned for the MTA experiments.

The thin film construction of the DESAL membrane inherently has a physical polarization. Coincidentally, the osmotic transport kinetics were found to be different from one side of the membrane compared to the other. Apparently, solute molecules do not have equal access to the thin film membrane pores from both sides of the membrane. The osmotic flow kinetics showed a lag when the solute was present on the non-thin film side of the membrane compared to the opposite orientation. The lag period was found to be reproducible, and to correlate with the physical orientation of the membrane. When the colligative solute was present on the thin film side of the membrane, no lag period was seen.

and the MTA functioned as intended. Figure 9 shows an example of the kinetic lag caused by the physical polarization of the membrane. In this experiment the membrane was oriented with the thin film side facing the lower fluid cell. The colligative solute was placed in the upper fluid cell, so the solute molecules were exposed to the thin film membrane through the polyester support. This transport behavior has been discussed with the membrane manufacturer, and additional types of membranes have been identified that may eliminate the osmotic flow polarization effect.

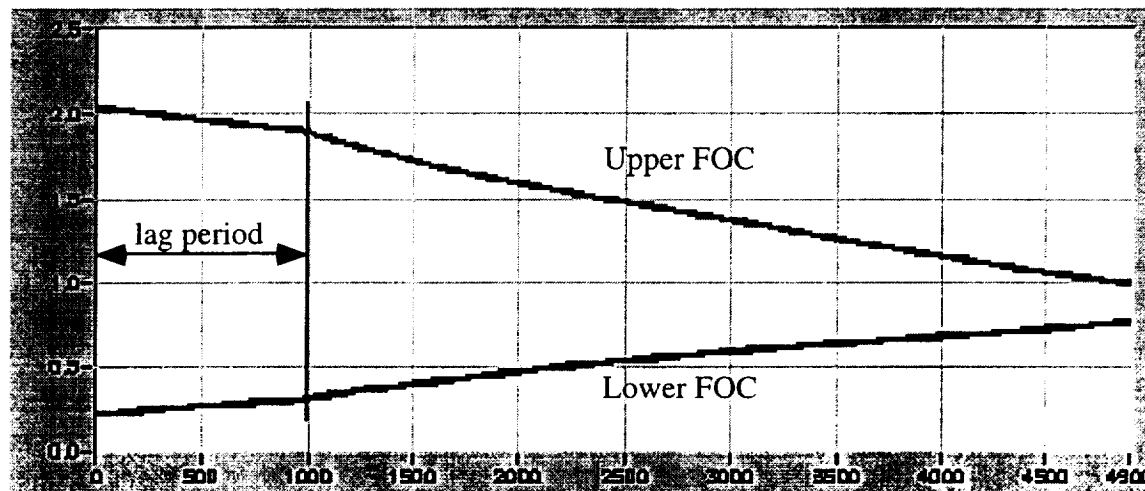


Figure 9 Osmotic Lag Caused by Physical Polarization of the Membrane

MTA OSMOSIS EXPERIMENTS

A series of osmosis experiments has begun to investigate the osmotic performance of various membranes. The objective of these experiments is to measure the solute dependent, membrane mediated flow kinetics. The membrane pillowing, orientation, and fluid leaks have affected the quality of the data in some of these experiments. The experiments have all taken place at room temperature. While the experiment is running, care is taken to minimize vibrations and movements that could mix the solutions in the MTA. A protocol was developed to characterize the experimental solutions. Most of the fluid characteristics are measured with a mass balance, a device that is highly dependent on gravity. Fluid properties that are characterized using gravity may exhibit unforeseen effects in the absence of gravity. In particular, the *specific gravity* of a solution seems to play a very important role in membrane mediated transport operations.

Osmosis experiments require long periods of time. When the experimental solutions are configured with solute on bottom (-1g) orientation, the boundary layer that forms in association with the membrane requires tens to hundreds of hours to reach steady state. The MTA sensors measure the dynamics of the osmotic boundary layer that forms in association with the membrane. Software modules have been developed to acquire the data from the MTA during the osmosis experiments, and to manipulate solutions within the Fluid Optical Cells. These Fluid Manipulation and Experiment software modules are used in sequence to initiate, acquire data, and terminate experimental operations.

Once the experimental solution has been prepared and characterized, it is transferred to either the Upper or Lower FOC using the Fluid Manipulation System, depending on the experiment gravity vector orientation. Deionized (DI) water is transferred into the opposite FOC to initiate the experiment. The current fluid cell design is not optimized for fluid filling and draining operations, and manual manipulation of the fluid cell assembly is

required to insure that complete filling occurs (no trapped bubbles). The initiation of an experiment corresponds to maximum hydrostatic pressure across the membrane, and maximum membrane pillowing in one direction. This configuration sets the membrane in an initially rigid position. As osmosis drives water through the membrane, the levels in the Volumetric Flow Sensors change, and are recorded as experimental data along with the ambient temperature. Refractive Index profile images are also acquired at regular intervals over the course of the experiment.

Fluid manipulation scripts have been developed to fill the Upper and Lower FOC's to pre-defined levels in preparation for an experiment. The FOC containing the solute is always filled to the minimal level (~0.2 cc), and the pure water FOC is filled to the maximal level. This initial configuration exerts the maximum hydrostatic pressure across the membrane at the start of an experiment, about 4 inches of hydrostatic head. The Fluid Manipulation System and associated software are described in a separate section of this report.

Experimental Solutions

The primary basis used to characterize the experimental solutions is weight percent (wt%), defined as dry solute mass relative to total solution mass (w/w). Table 2 lists the procedure is used to prepare and characterize the experimental solutions.

Table 2 Experimental Solution Preparation Procedure

<i>Weight percent measurements</i>		
1) Define approximate solute weight percent (wt%)		
2) Weigh out dry solute mass appropriate for 100 grams total solution		
3) Record dry solute weight		
4) Fill beaker to about 100 ml using degassed, deionized (DI) water		
5) Record total solution weight		
6) Stir solution until all solute is dissolved		
<i>Specific Gravity and Refractive Index measurements</i>		
7) Fill 5.00 cc volumetric flask to mark with solution		
8) Measure and record mass of 5.00 cc of solution		
9) Measure and record solution refractive index (Brix)		
10) Transfer solution to labeled bottle for storage & experimental use		
<i>Solution Properties characterization</i>		
11) Calculate solution properties using the following formulas:		
$\text{wt\%} = 100 * (\text{mass dry solute}) / (\text{mass dry solute} + \text{solvent})$		[dimensionless]
$\text{rho} = (\text{mass solution in volumetric flask}) / (5.00)$		[g/cc]
$\text{conc} = (10^6) * (\text{wt\%} / (\text{rho} * 100)) / (\text{solute MW})$		[mol/liter]
$\text{Refractive Index} = (1.33305 + 0.0013728 * \text{brix} + 0.00000736914 * \text{brix}^2)$		

A Mettler PM2000 analytical balance was used for all mass measurements. The balance measures to a precision of 10 mg, and is in an annual calibration cycle. Refractive index measurements were performed using a Leika 0-30° Brix hand-held refractometer. All measurements and experiments were performed under ambient (room temperature) conditions. A 5.00 cc volumetric flask was used to measure solution specific gravity (termed rho). The flask has been periodically calibrated by filling to the mark with DI water, and measuring the mass of the contained water. Each time the contained mass was found to weigh 5.00 grams. The solution specific gravity is calculated as the ratio of solution mass to that of the same volume of water at the same temperature. The Refractive Index polynomial was taken from a regression fit to data for sucrose solutions at 22°C provided by the LMA Metrology Dept. Solute molecular weights were taken from manufacturers specifications and Material Safety Data Sheets (MSDS).

Polyethylene Glycol (PEG) solutes cover a range of molecular weights. The molecular weight value used for calculation and labeling represents an average that corresponds to the number of polymer subunits that are associated to form PEG molecules. A range of molecular weight solutions have been characterized using this procedure. Figure 10 (a) shows how the solution specific gravity correlates to weight percent. Figure 10 (b) shows the correlation between the solution specific gravity and refractive index as measured using the hand-held refractometer.

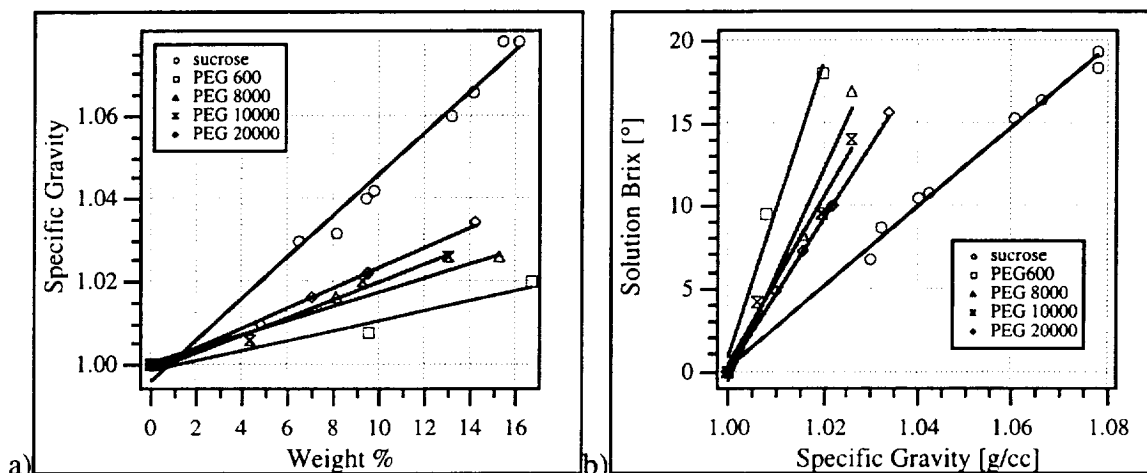


Figure 10 MTA Experimental Solution Characteristics Relative to Weight Percent.
 (a) Solution Specific Gravity as a Function of Weight Percent
 (b) Solution Brix as a Function of Specific Gravity

The refractive index of each experimental solution is shown to be a linear function of the specific gravity. This mathematical relation makes it possible to calculate solution specific gravity directly from the refractive index profile images. This calculation is performed in the Refractometer Image Processing software, described in another section of this report. These relations among fluid properties are also used in the development of the MTP Analytical Model, as described in that section of this report.

Experimental Data Acquisition

The user interface for the MTA Experiment data acquisition software has been upgraded, and is fully automated. The mass transport kinetic data are measured and acquired using this software during an experiment. When an experiment is begun, the user is prompted for datafile disposition information for both the VFS data and the refractometer images (separate files for each). The experimental data acquisition activity is initiated upon completion of the various dialogs. Figure 11 shows the user interface panel for experimental data acquisition and status display.

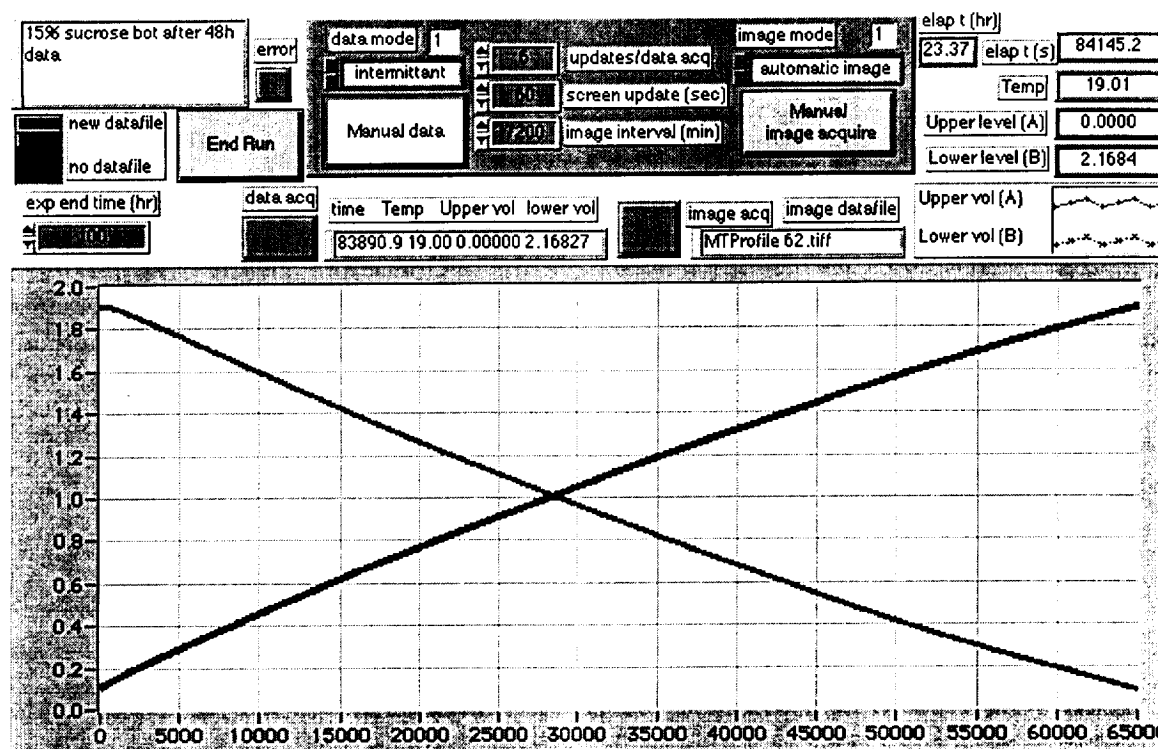


Figure 11 User Interface Panel for Experimental Data Acquisition

The intervals for data acquisition are user set through the front panel controls. The values for these variables can be changed during an experiment to tailor the acquisition intervals to the dynamics of the boundary layer formation. Data file identification, experiment elapsed time, current VFS levels, and temperature data are also displayed on the control panel. The graph in the lower part of the display panel shows the VFS data acquired for both FOC's as a function of elapsed time intervals. The experiment ends when the elapsed time is greater than the Experiment End Time value, or by manually clicking the End Run button. When the experiment is terminated, the datafile is closed and execution of the program ends. The experimental data is stored in files on the computer hard disk for later analysis. The data is formatted as tab delimited text, and can be accessed from many different applications for manipulation, graphing, editing, and analysis.

The experiment software has also been upgraded to include an interface to a time lapse VCR and ASCII character generator. This allows the refractive index profiles generated during an experiment to be recorded in time lapse form, with the experiment elapsed time, VFS, and temperature data superimposed over the refractometer images. This character generator interface and time-lapse VCR link were developed in association with the DC-9 Flight Experiment software, described in another section of this report.

Experiments were conducted with the colligative solution in both orientations relative to the gravity vector. The presence of the colligative solution in the upper fluid cell (+1g) inhibits the formation of a membrane mediated boundary layer, and the colligative solute positioned in the lower fluid cell (-1g) enhances the formation of the boundary layer. The fluid cell opposite to the colligative solute is always filled with pure water as the mobile solvent. These two configurations show very different transport kinetics.

Solute on Top (+1g) Experimental Results

This experiment was performed with the colligative solution in the Upper FOC. The thin film side of the DESAL RO membrane was also facing upwards, toward the colligative solution. In this membrane orientation there is no lag period present from the membrane physical polarization effects. Figure 12 shows a plot of raw data from this osmosis experiment. The colligative solution used was 10 wt% PEG (molecular weight 20,000), located in the upper fluid cell (+1g orientation). Deionized water was used in the lower fluid cell, and osmosis acted to drive the water from the lower cell into the upper cell. The VFS data for each fluid cell is shown on the left axis, and the ambient temperature on the right axis.

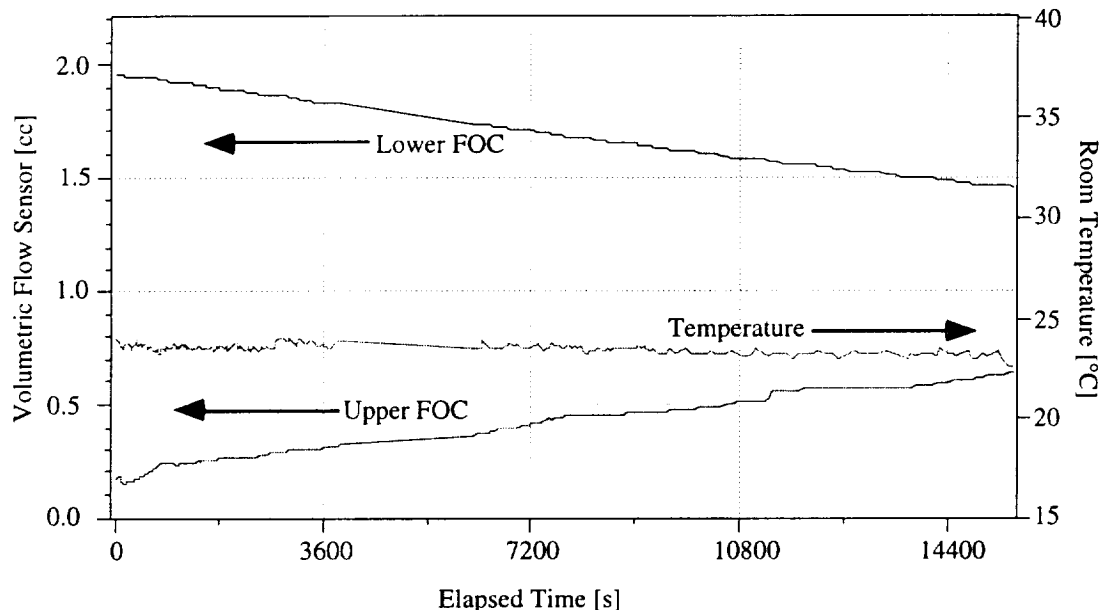


Figure 12 Raw Experimental Data From 10 wt% Polyethylene Glycol (PEG 20,000) in the Upper FOC (Solute on Top, +1g)

There is a wealth of information regarding the experimental solutions shown in this VFS data. Since no mass is created or destroyed within the MTA, the mass of water that moves through the membrane from one FOC to the other should balance out, within the limits of the sensor calibration. However, the fluid/solvent dissolution process is nonlinear, and volume effects associated with dissolution of the solute material in water occur within the fluids. These effects can be seen in the VFS data on the solution side (Upper FOC) of the membrane as small bumps in the fluid volume kinetics. Figure 13 shows the absolute value of the delta volumes calculated for each FOC as a function of time. The delta volume is simply the absolute value of the VFS data at an elapsed time minus the volume at time 0 $|V_t - V_0|$. Inspection of the delta volume data for the solute side (Upper FOC) shows that the fluid volume undergoes episodic transients that show the fluid dissolution effects. The pure water (Lower FOC) data shows a smooth curve that reflects the relatively constant solvent flux driven by osmosis through the membrane. The +1g orientation acts to mix the solute in the upper FOC, and the uneven nature of the flow data reflects the nonlinear dissolution process. The inverse orientation (-1g) solute side flow data do not show this uneven behavior. In the -1g orientation, gravity acts to enhance the formation of the fluid boundary layer, and the mixing phenomena are absent.

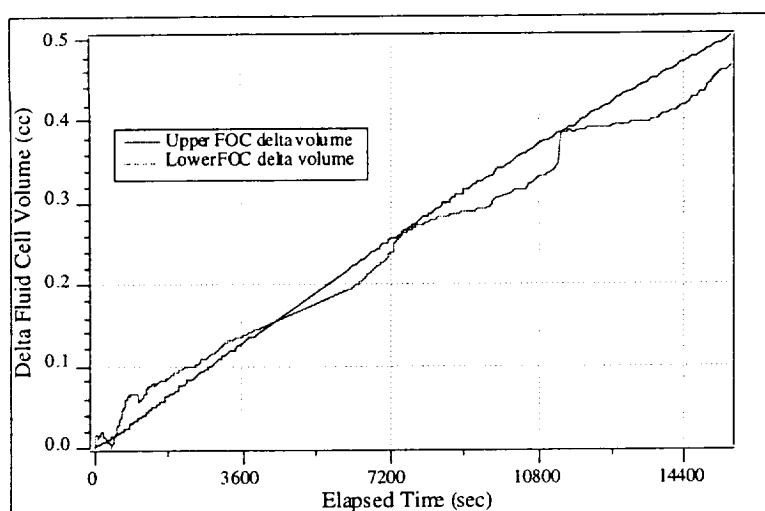


Figure 13 Delta Volume VFS Data for 10 wt% Polyethylene Glycol (PEG 20,000) in the Upper FOC (+1g, solute on top)

Mass flow data for determining the osmotic flow kinetics is most reliable when taken from the FOC that contains only water. This data is the most reliable because the VFS sensors were calibrated using pure water, and no volume dissolution effects are present in the pure water fluid cell. In a leak free system, the flow rate through the membrane can be calculated from the experimental data as the first derivative of the VFS readings with respect to time (dV/dt). Analysis of the VFS data in this way is useful for several aspects of experiment analysis. The most important of these is the indirect determination of the solute concentration directly adjacent to the membrane, the concentration that drives the osmotic transport process. The flow rate of water through the membrane is directly proportional to this solute concentration. This extrapolation provides a measure of the boundary layer end point for use in the MTA Analytical Model. The extrapolated data can also be compared with the refractometer images as an additional measure of the driving chemical potential. The refractometer images are limited by the thickness of the Viton seals that secure the membrane in place and prevent fluid leaks. The fluid directly adjacent to the membrane is obscured from the refractometer beam by these seals, and an extrapolation is necessary to estimate the solute concentration hidden by the seal. This analysis technique offers an independent determination of solute concentration directly next to the membrane.

There are additional advantages to processing the VFS data in this way. The abrupt data offsets that occur when the membrane moves because of hydrostatic pressure and pillowing effects are shown as large (transient) changes in the otherwise monotonically changing flow rate. Thus, the membrane movement effects are easily separated from the osmotic transport measurements.

Refractive index profile images were acquired during this experiment, and are shown in Figure 14. The convective actions produced by gravity act to mix the solution in the upper fluid cell over time, and no significant differences are shown among these images. The gravity vector is orientated toward the bottom of the page for all the images shown, and the experiment elapsed time in seconds is shown in each of the image frames.

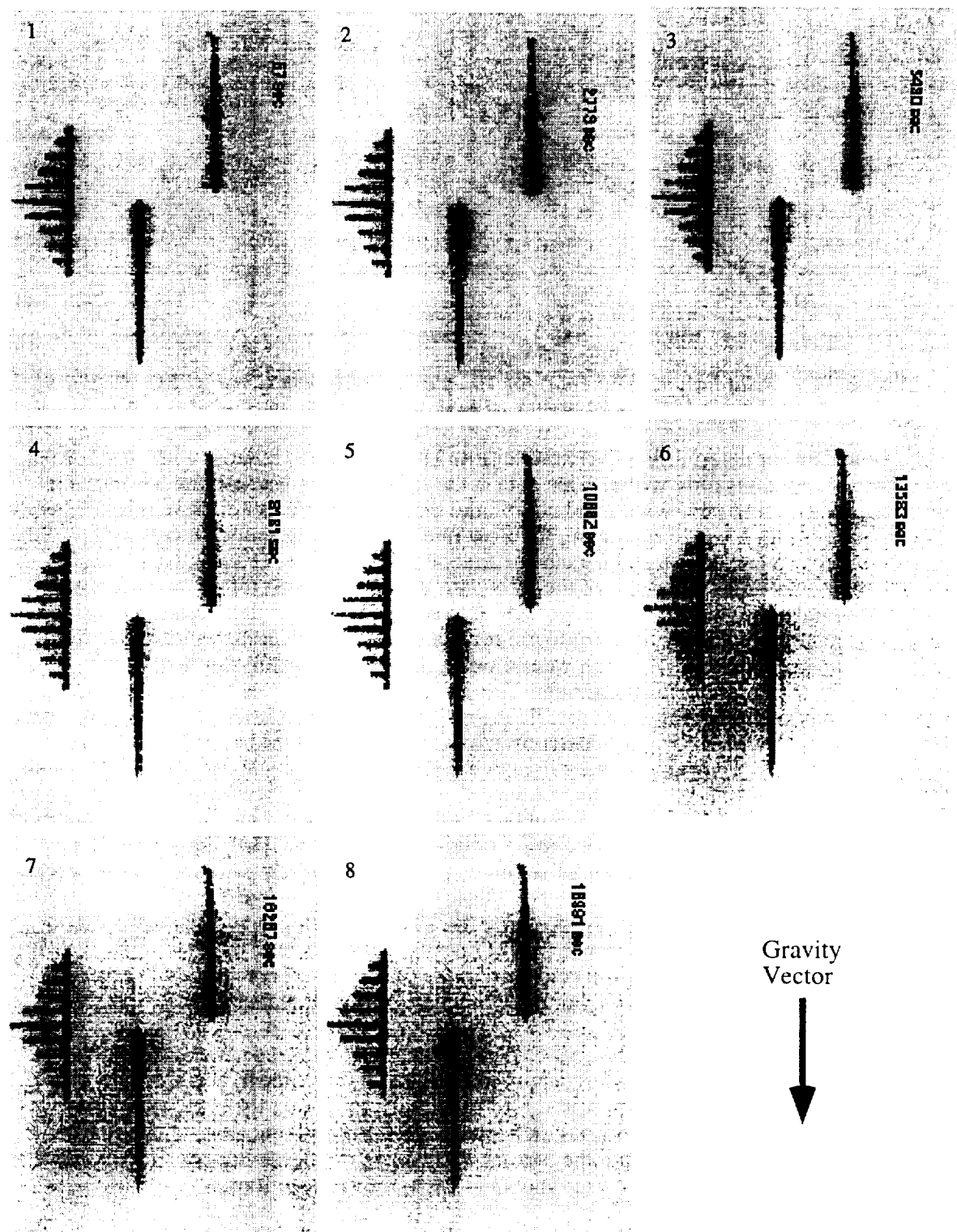


Figure 14 Refractive Index Profile Images for 10% PEG 20,000 in the Solute on Top Configuration (+1g) Osmosis Experiment.

Solute on Bottom (-1g) Experimental Results

This osmosis experiment was performed in the opposite gravimetric orientation, and used 8% PEG (mol wt: 20,000) in the lower fluid cell as the colligative solute. The DESAL RO membrane was used in the experiment, and the thin film side of the membrane was again oriented towards the lower FOC to prevent osmotic lag. A gravimetrically stable fluid boundary layer was created in association with the membrane that altered the kinetics of mass transport as the experiment proceeded. Raw data from an inverted orientation osmosis experiment is shown in Figure 15. In contrast to the +1g orientation, the VFS data for the solution side (lower FOC) is shown to be smooth, with no dissolution effects apparent. The flow rate of water through the membrane changes over time due to the formation of the boundary layer next to the membrane.

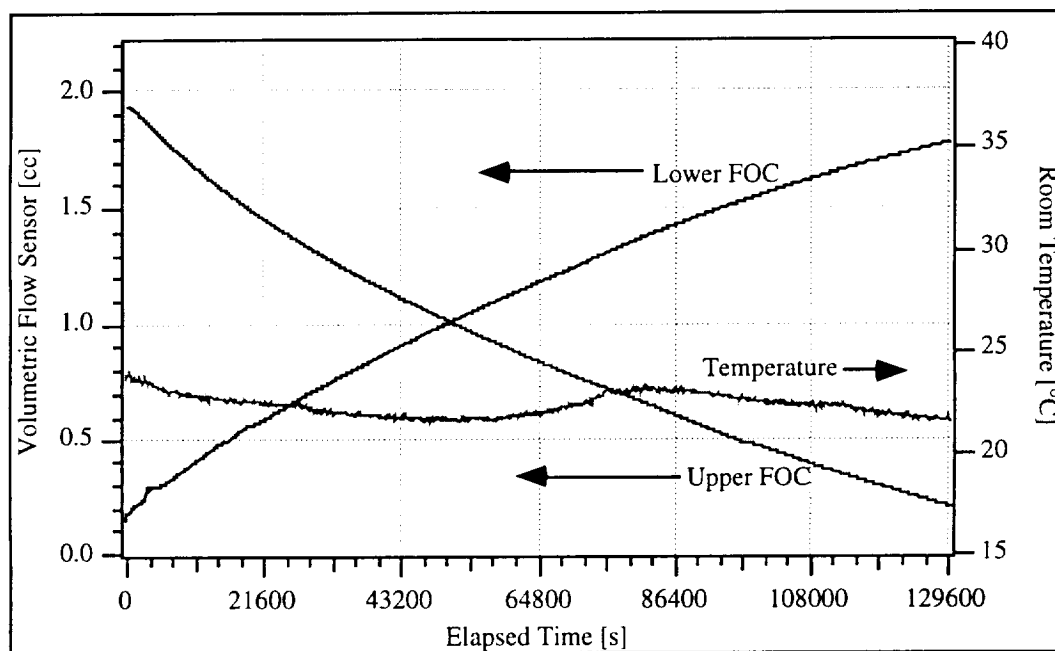


Figure 15 Raw Data from Inverted Orientation Experiment. 8% PEG (mol wt: 20,000) in the Lower FOC (Solute on Bottom, -1g)

Figure 16 shows the differentiated VFS data from this experiment (8% PEG 20,000 on bottom) for the flow rate of solvent flow out of the Upper FOC. The flow values are negative because the solvent (water) was flowing out of the upper fluid cell, into the lower cell. Each data point represents one calculated dV/dt value, and the line a moving average of the data calculated over 100 successive data points. The solvent flux through the membrane is approaches zero as the boundary layer develops, inhibiting further osmosis.

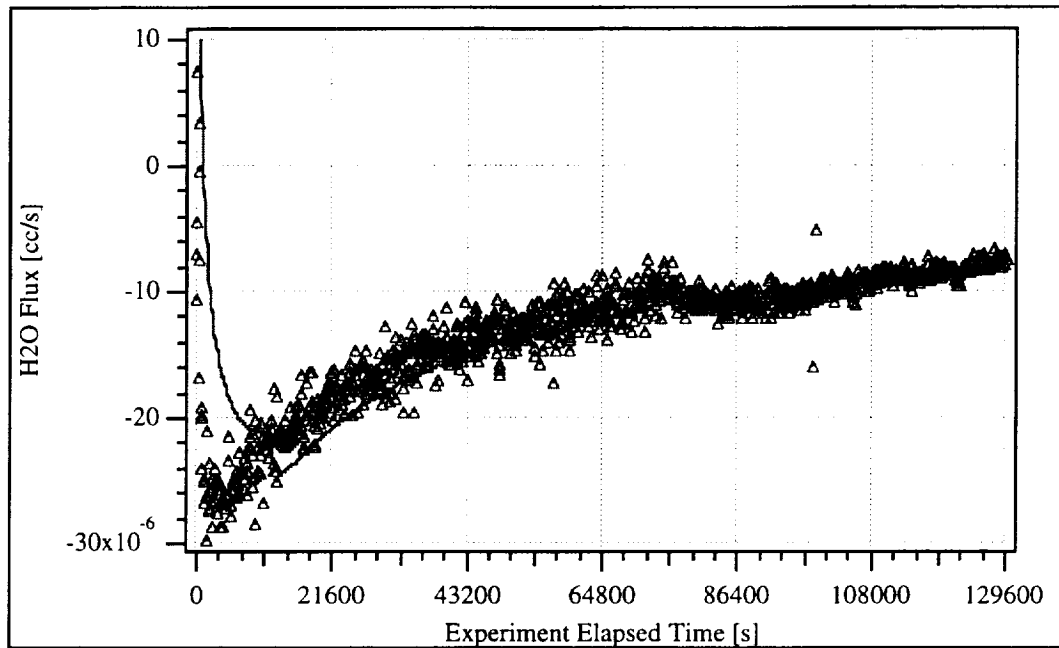


Figure 16 VFS Data from 8% PEG 20,000 on Bottom Osmosis Experiment
Differentiated with Respect to Time (dV/dt)

Figure 17 shows the series of refractive index profile images acquired during this osmosis experiment (8% PEG 20,000 on bottom). The images represent the raw data that has been processed to show the (red) 8 bit grayscale values extracted from the color images. Each image represents a snapshot of the fluid profile present within the fluid cells at the elapsed time shown in the upper corner. The developing boundary layer that forms in response to the osmotic transport of water into the lower fluid cell is clearly shown. As before, the gravity vector is orientated toward the bottom of the page, with the calibration figure to the left of the refraction beam profile.

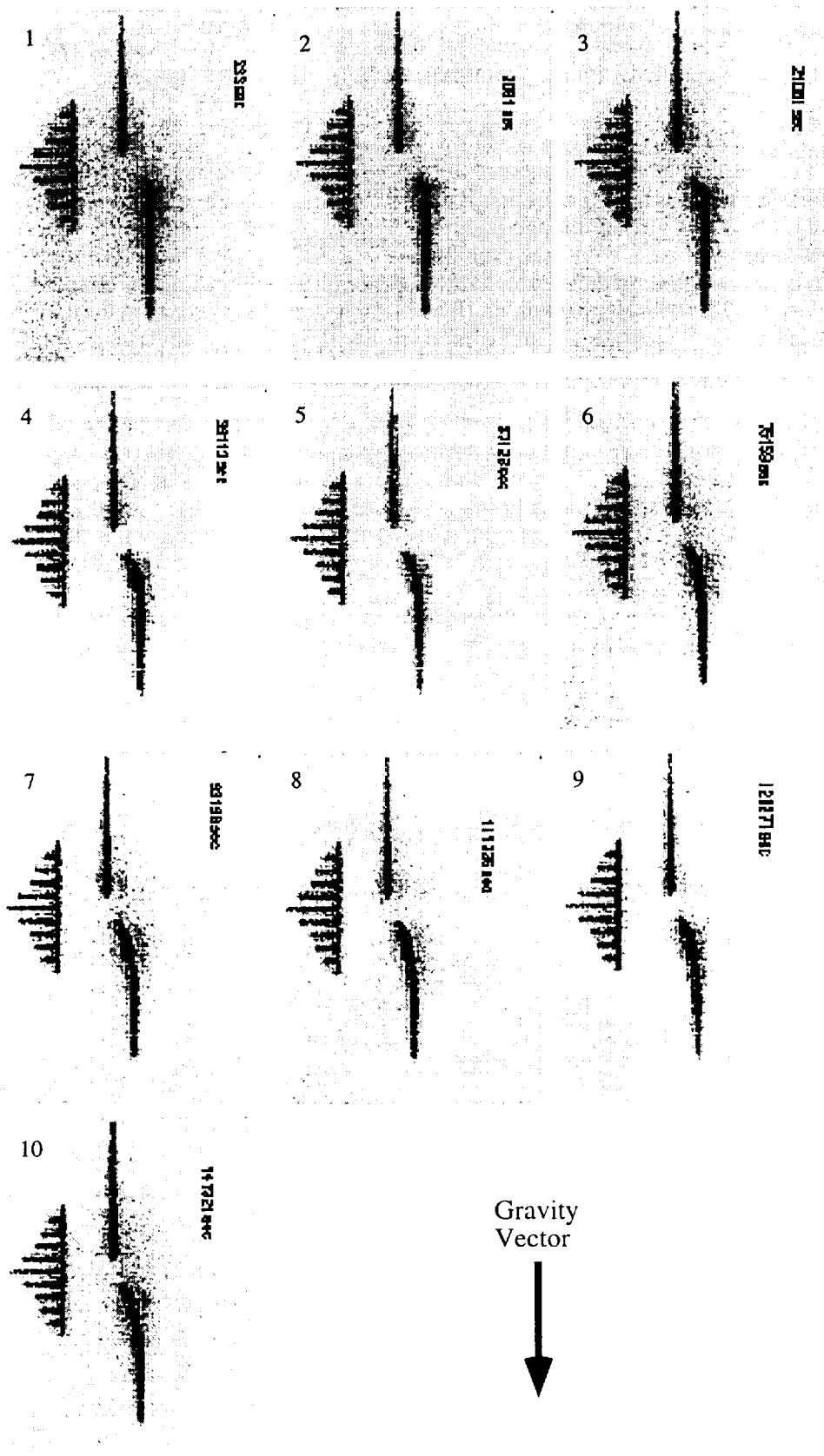


Figure 17 Refractive Index Profile Images Acquired During the 8% PEG 20,000 on Bottom Configuration (-1g) Osmosis Experiment.

MTA FLUID MANIPULATION SYSTEMS (FMS) DEVELOPMENT

The Fluid Manipulation System was developed to sequence fluid valves and enable automated fluid transfers within the MTA. The use of the FMS became necessary to eliminate convective interference's that were occurring in the lower fluid cell. During osmosis experiments where the colligative solution was positioned in the lower fluid cell, it became apparent that gravity induced convective flows were mixing the fluid boundary layer as it developed adjacent to the membrane. The MTA had to be reconfigured to eliminate the convective interference, a development that required major changes in the fluid system design. The new instrument configuration represents a quantum evolution in the MTA fluid handling capabilities, and is more flight like than the previous fluid configuration.

Initially, the Volumetric Flow Sensor (VFS) for the lower FOC was connected to the fluid cell outlet port nearest the membrane. As osmosis caused water to flow through the membrane, undiluted solute contained within the VFS (located physically above the level of the membrane) was of higher density than the pure water next to the membrane, creating a convectively unstable fluid arrangement. Convection acted to stabilize the fluid layers, and mix the developing boundary layer with higher density solute that was contained within the VFS. This mixing action perturbed the boundary layer structure and altered the kinetics of flow through the membrane. A redesign effort was initiated to prevent this from occurring. Figure 18 shows the MTA in the new configuration, complete with the fluid switching valves.

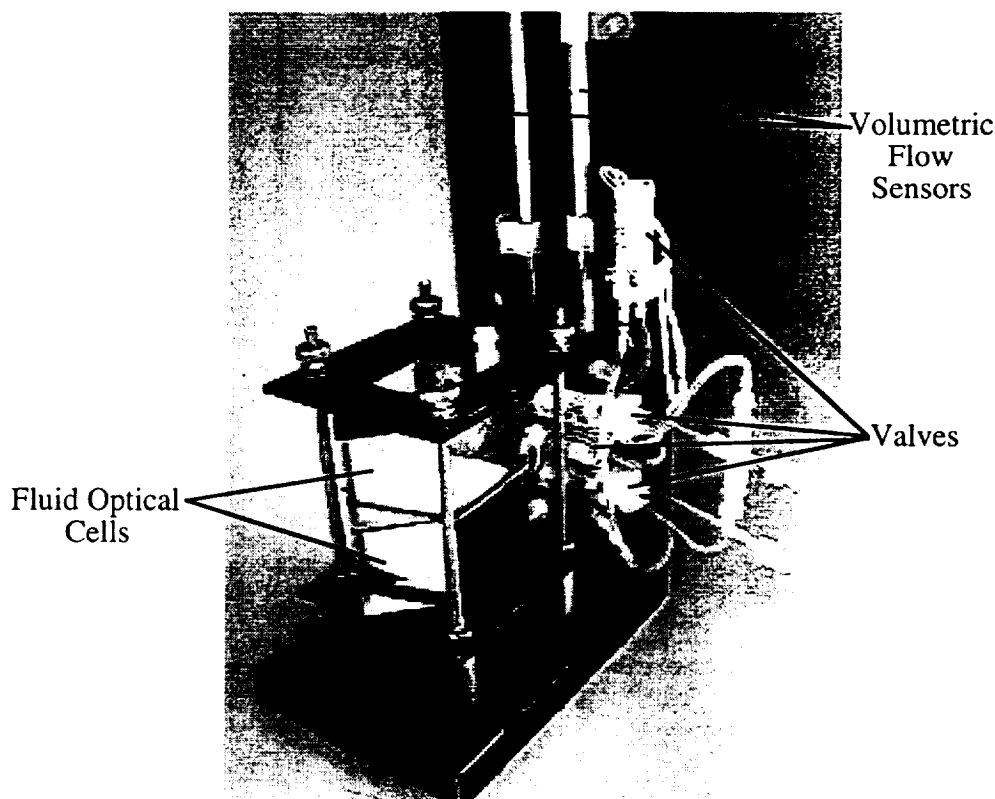


Figure 18 Reconfigured MTA with Fluid Switching Valves

The new configuration alters the relative position of the VFS in the lower fluid cell, and establishes a symmetry around the membrane with respect to the VFS. This relative positioning insures that no gravimetrically unstable fluid layers are created during the

osmosis experiments. Simply stated, the Volumetric Flow Sensors are now located at the farthest points from the membrane in both the Upper and Lower FOC's. The new configuration is more complex than the prior arrangement, and requires valves to insure that fluids flow sequentially into the FOC's and VFS in preparation for an experiment.

Both of the fluid cells must be filled from the lower (inlet) port in a 1g environment. To accomplish the filling operation, the valves are sequenced to first direct the experimental fluids into the upper fluid cell and VFS, then into the lower fluid cell and VFS. The position of the upper VFS remains at the (upper) outlet port for the upper cell, and is naturally filled from the bottom. The lower VFS was moved to a position near the lower fluid cell inlet port, and requires valves to insure that the fluid cell is filled prior to the VFS. Four valves are required for these fluid manipulations. The valves are electrically operated, and a collection of electrical interface circuits were developed to allow computer actuation of the valves in sequences appropriate for the fluid manipulations. The MTA fluid flow schematic diagram is shown in the Fluid Manipulation Software section of this report.

The valve electrical interface was extended to include the circuit drivers for control of the peristaltic pumps and the refractometer laser. A modified transistor switching circuit was developed to amplify the TTL level signals generated by the computer into a form appropriate to drive the valves, laser, and pump control circuits. Circuits of this type were developed for the laser, both pumps, and eleven valves. The interface circuitry also includes an LED display to indicate the energized state of each drive circuit (valve and pump operations), and a manual override switch for laser control. Figure 19 shows the valve, laser, and pump electrical circuits as consolidated into a single circuit box. The two parts shown fit together to form an integral unit that functions to perform the interface operations, connect to the instrument and computer, and display the actuation state of each valve.

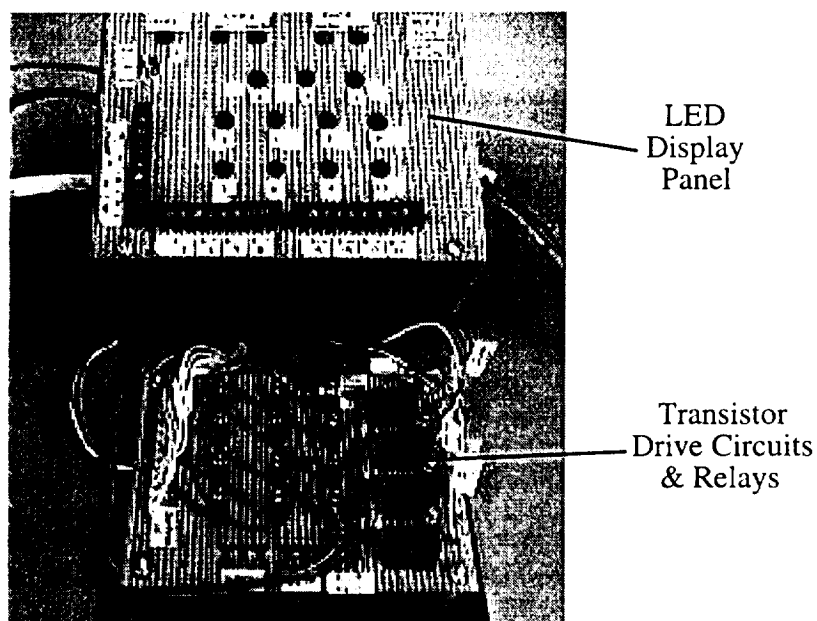


Figure 19 MTA Valve, Laser, and Pump Electrical Interface Circuitry

After a few months of FMS operation, it was found that some of the valves were malfunctioning. The problem was discovered while filling the lower Fluid Optical Cell with a high viscosity solute (PEG 20000) in preparation for an experiment. This malfunction occurred while the membrane seal assembly was in the latex and Viton gasket

configuration, and prompted further development of the seal. The lower fluid cell outlet valve had become stuck in the closed position while the fluid pumps were pumping solute in, and caused a higher than normal pressure to be exerted across the membrane. The pressure caused the membrane to come loose from its seat between the Upper and Lower FOC's, a "blown membrane". It was later determined that the valve malfunction did not happen all at once, it occurred gradually over the course of several experiments. Initially, the increased pressure caused the membrane to be displaced within its seal more than usual. The excessive membrane pillowing that was observed was attributed to the high viscosity solute that was being used. Eventually the valve became completely stuck in the closed position, and the membrane came loose from its seal between the FOC's. Several fluid manipulations, blown membranes, and FOC rebuild cycles occurred before it was realized that the valves were malfunctioning.

The valve problem was investigated and all valves in the MTA tested. Some of the MTA valves showed leakage in "closed" paths, while other valves would not switch fluid paths when actuated. In all cases the software and electrical circuitry showed no problems. In discussions with the valve vendor (Lee Valves), it was determined that a material used to construct the valve seat (Neoprene) is not compatible for continuous contact with aqueous solutions. Apparently, Neoprene has a tendency to absorb small amounts of water and swell, a property that is not listed in the materials selection section of the Lee catalog. When the Neoprene valve seat material swells, it can become lodged within the actuation path, or not seat completely against the fluid valve ports. These valves are then prone to leakage and/or sticking in open or closed positions. The malfunctioning valves seem to become operational again once the absorbed water has evaporated from the Neoprene seat material.

The Lee Valve Company recommended replacement valves that have valve seats constructed using an aqueous compatible material (Teflon). New valves were ordered to replace the current valves, but have not yet been received. In the interim, three of the four malfunctioning valves have been replaced with spares (also Neoprene valve seats). This allows the MTA experiments to continue until the new valves are received. The initial (Neoprene seat) valves worked fine for about three months before the malfunction occurred. The new replacement valves should be received before the spare valves malfunction.

FMS SOFTWARE DEVELOPMENT

Software was developed to sequence the pump and valve operations, and to orchestrate complete fluid manipulation operations within the MTA. LabVIEW was used to create the MTA Fluid Manipulation System program, a graphical, object oriented, instrument control application. The Fluid Manipulation System software is functional through either script driven (automatic) or manual operation. Manual operations are accomplished through a Graphical User Interface that allows valves to be actuated through mouse click operations, and graphically displayed on the MTA flow schematic. The display shows fluid paths, valve positions, actuation states, pump status, and VFS data. Figure 20 shows the Graphical User Interface for status display and manual manipulation of the MTA valves.

The valves shown in the figure are actuated by simply clicking on the valve using the computer mouse. When actuated, the computer issues the command to change the valve state, and updates the flow schematic to show the fluid path associated with the current valve state. The peristaltic pump indicators show the direction and speed of each pump, and flash when the pumps are running. The fluid volume contained within each of the Volumetric Flow Sensors is also displayed, and continually updated as the program executes.

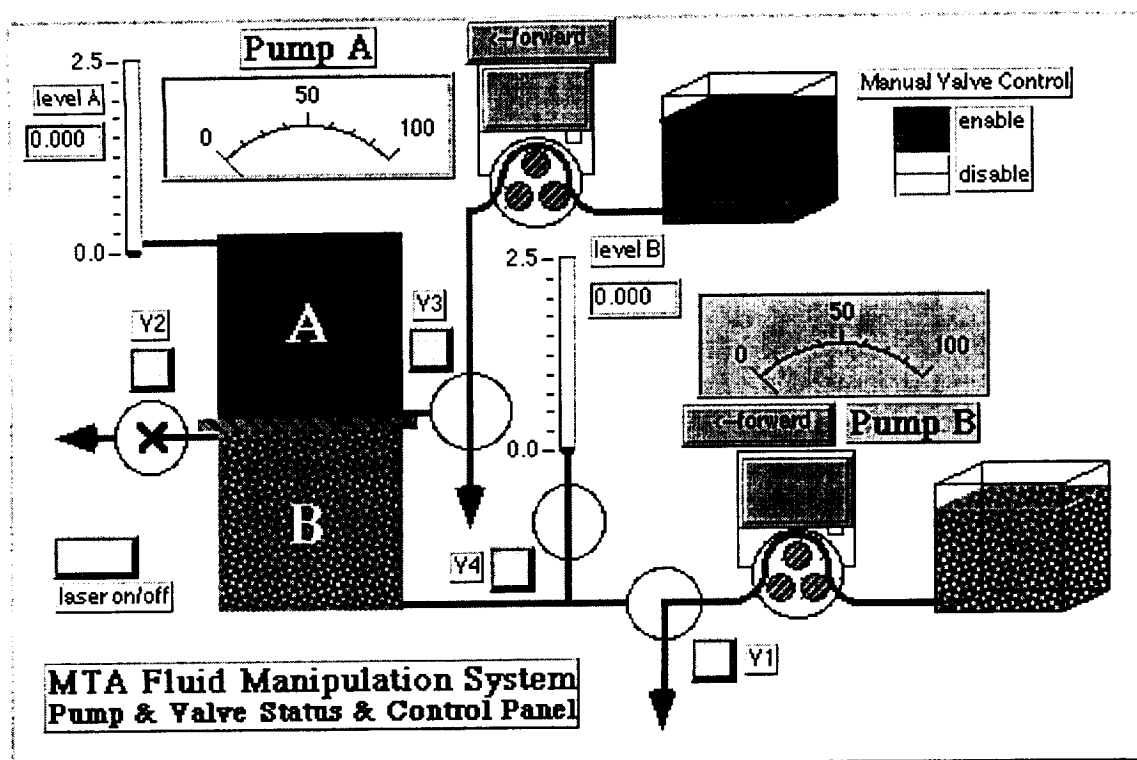


Figure 20 MTA Fluid Manipulation System Graphical User Interface

The fluid manipulation scripts for automated sequences of operations consist of independent lines of tab delimited ASCII text. These lines can be generated using a word processor, spreadsheet application, or LabVIEW editor. Sequences of the script lines are put together to form complete fluid manipulation scripts. Scripts have been written to perform all of the fluid manipulation functions within the MTA, and include fluid cell filling and draining operations, fluid cell and tubing purges, refractometer calibration, and Volumetric Flow Sensor calibration.

Execution of the fluid scripts is accomplished through a hierarchy of software modules, or subroutines. A script interpreter was developed that performs calls to the various subroutines in the timed, sequential order specified by the script. Subroutines have been developed to manipulate valve states, pump volumes of solutes in to or out of either fluid cell, and to perform closed loop filling operations that use the Volumetric Flow Sensors as the feedback element. The software was constructed in an object oriented hierarchy, where the fluid manipulation functionality is coded into lower level subroutines that are callable through the script commands. The scripts also allow each operation to be sequenced in time. An example script command is shown below in Figure 21, where each (tab delimited) text column is associated with a specific function through the script interpreter.

4	5	1.0	75	Wait 4 sec then Fill Upper FOC to 1.0cc @ 75%
---	---	-----	----	---

Figure 21 Example Script Line to Command Fluid Operations (Tab Delimited Text)

This script line commands the Fluid Manipulation System to perform a closed loop filling operation of the Upper FOC, filling the fluid cell until the Volumetric Flow Sensor indicates a contained volume of 1.0 cc. The 5 indicates to the script interpreter that a closed loop level filling operation is to take place in the Upper FOC after an elapsed time of 4 seconds. At that time, the volumetric flow sensor is to be filled to 1.0 cc volume using a

pumping rate of 75% of maximum. The comments are the last entry in each script line to document functionality and enable script debugging. A complete listing of script line interpretation syntax is shown in Table 3.

Table 3 MTA Fluid Manipulation Script Command Interpretation Syntax

VALVE MANIPULATION SYNTAX:				
<u>et</u>	<u>port</u>	<u>line</u>	<u>state</u>	<u>comment</u>
time	1-2	0-7	0-1	single bit write
time	1-2	0-255	-1	8 bit port write
port 1 (B) Valve Control				
0 1	bypass/fill		V1=Lower (B) fluid cell input valve	
0 2	closed/open		V2=Lower (B) fluid cell outlet valve	
0 4	bypass/fill		V3=Upper (A) fluid cell input valve	
0 8	open/closed		V4=Lower (B) level sensor access valve	
port 2 (C) Pump & Laser Control				
0 1	stop/start		Pump A control	
0 2	fwd/rev		Pump A direction	
0 4	stop/start		Pump B control	
0 8	fwd/rev		Pump B direction	
0 16	off/on		laser control	
FLUID MANIPULATION COMANDS:				
<u>et</u>	<u>instr</u>	<u>volume</u>	<u>speed</u>	<u>comment</u>
time	3-4	\pm vol	0-100	pump specified volume
		3=Upper FOC (A) 4=Lower FOC (B)		
<u>et</u>	<u>instr</u>	<u>volume</u>	<u>speed</u>	<u>comment</u>
time	5-6	setpt	0-100	fill fluid cell to specified setpoint
		5=Upper FOC (A) 6=Lower FOC (B)		
<u>et</u>	<u>instr</u>	<u>DAC</u>	<u>volts</u>	<u>comment</u>
time	7	0-1	0-10.0	set DAC pump drive voltage
		1=Upper FOC (A) 0=Lower FOC (B)		

Scripts have also been generated to control the valve sequences and pumps for the upcoming DC-9 Flight Experiment. This software is described in the DC-9 Experiment description section of this report.

REFRACTOMETER IMAGE ANALYSIS SOFTWARE DEVELOPMENT

An upgraded version of LabVIEW (4.0) has recently become available, and has enabled the MTA image processing software to be upgraded into a user interactive form. This is possible due to the compatibility of this version of the software with the C++ compiler used to code the original image processing algorithms, as described in the first MTP Technical Report (May 1996).

The upgraded MTA image processing software allows individualized analysis of the refractometer images acquired during osmosis experiments. This program runs within the LabVIEW environment instead of as a stand-alone application, and takes advantage of the built in graphics capabilities and user interface. The program includes a complete Graphical User Interface (GUI) that enables the user to process and analyze each aspect of the refractive index profile image separately, and allows iterative optimization of input threshold values to obtain the highest quality interpretation of the imaged calibration pattern and refractive index profiles. Figure 22 shows the Graphical User Interface for the interactive image processing program.

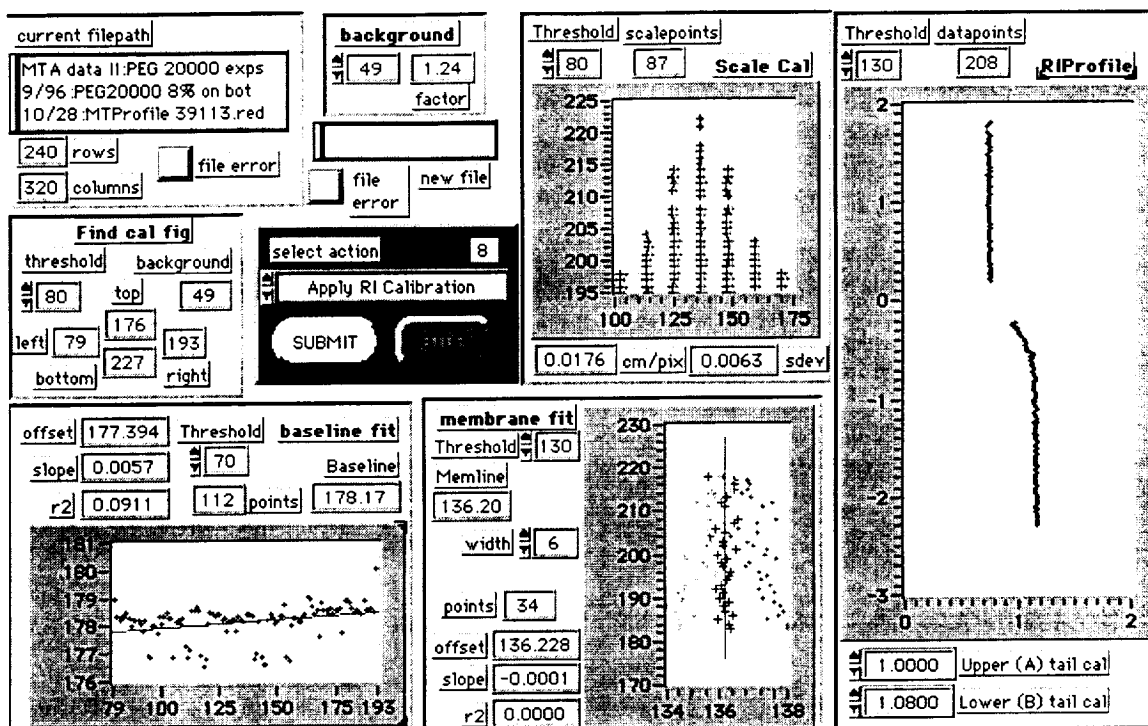


Figure 22 Graphical User Interface for Interactive Refractometer Image Processing

Each of the boxes in this panel is associated with a different aspect of the image analysis. Starting from the upper left, the image file is specified through a dialog and displayed here. The "Find cal fig" box functions to locate the calibration figure on the image, and specifies a region of interest for further analysis. The image background is determined from the lower left hand corner of this region of interest, and subtracted from each pixel in the image. The entire image grayscale is then re-stretched to cover the full 8 bit intensity range to enhance the contrast between the laser lines and the background image levels. The "baseline fit" box performs a linear regression analysis to define the refraction baseline from which all refraction distances are measured. The graph shows a plot of the location of the calibration baseline in terms of pixel address on the image. The "membrane fit" box performs a similar analysis to define the plane of the membrane perpendicular to the refraction baseline. The graph is a plot of the starting, weighted average, and ending pixel addresses associated with the central spike in the calibration image. The "Scale Cal" module performs a statistical analysis on the intervals between the calibration grid lines, and calculates the mean and standard deviation of the interval distribution. The graph shows the intervals that were analyzed in terms of starting, weighted average, and ending line pixel addresses for the input intensity threshold value. The RIprofile graph shows the refraction beam profile as scaled to the refraction baseline and membrane planes. The profile data is output to a separate file for further analysis as paired terms for membrane distance and refraction offset distance, each data pair corresponding to a single pixel entry of the refraction beam in the profile image.

The program was written using the algorithms written in C++ that had previously been used in the stand alone application described in the first MTP Technical Report (May 1996). These program modules were modified into a library of C functions, and incorporated into a series of LabVIEW Code Interface Node (CIN) program elements. A CIN is a mechanism that allows compiled C code to be executed from within the LabVIEW environment as a callable subroutine. The series of CIN's were embedded into Virtual

Instruments (LabVIEW subroutines), and structured together to enable end to end processing of the MTA refractive index profile images. This custom processing ability allows precise dimensional calibration of refractometer images by processing the images to correct for background level and laser intensity variations over the entire image. Figure 23 shows the virtual instrument front panel for one of the CIN's used in this program. This subroutine exists in the computer memory as compiled source (object) code, and is linked through the virtual instrument subroutine to the LabVIEW environment.

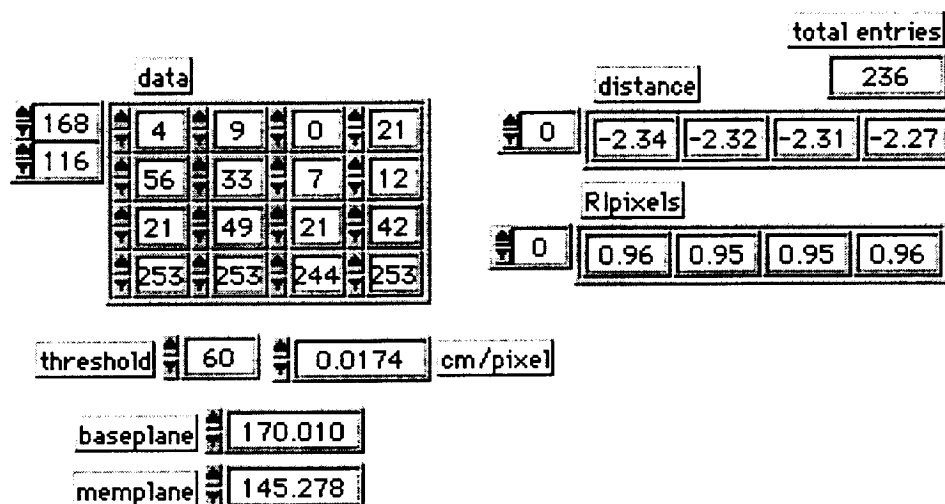


Figure 23 Code Interface Node (CIN) Virtual Instrument. This CIN is used for calculating the refractive index profile values in an MTA refractometer image.

The displays shown in the figure represent the inputs and outputs of the subroutine for calculating the refractive index profile data points. The image data, cm/pixel, baseplane, memplane, and threshold are inputs, and the distance, Rpixels, and total entries are outputs. Within this subroutine, each value calculated in the refractive index profile corresponds to an individual pixel in the image, with the numeric value dependent on the scale calibration and desired output units. The display labeled "data" is a two dimensional array that represents the 8 bit grayscale value (0-255) of each pixel in the image being processed. The "total entries" display indicates how many pixels were identified in the refractive index profile shown in the image, for the input "threshold" value. This threshold was found to be the key parameter associated with this program module, and defines the minimum grayscale value criteria for evaluating the refractive index profile. The "distance" and "Rpixels" displays each represent a one dimensional array of paired numeric data that define the refractive index profile. The distance data are in units of centimeters measured perpendicular to the plane of the membrane, and the Rpixel data is measured in the desired output dimensional units (density, RI, Brix°, or Weight%). The MTA refractometer calibration coefficients are incorporated in this routine, and used to scale the output data through the procedure described in the MTA Refractometer Calibration section of this report.

The interactive nature of the program enables each of the image processing modules to be optimized, a process that is somewhat time consuming. Using this program on a series of images allowed the key image processing parameters to be identified. These parameters were then programmed into a separate, batch mode program to allow automated processing of a series of images. Optimization is performed on each of the key parameters by analyzing each image over a large range of parameter input values and monitoring the

quality of the analysis as shown by the output variables. For example, the magnitude of the standard deviation from the mean is used to optimize the scale calibration analysis. The threshold value that yields the lowest standard deviation is then identified and used to calculate the dimensional scale of the image. This automatic processing program is an effective method for processing the large quantity of data that is generated in the osmosis and refractometer calibration experiments. The automatic program does not always produce the best data, however. Some images do not work well with this analysis and must be analyzed manually using the interactive program to attain optimal results.

MTA REFRACTOMETER CALIBRATION

A calibration procedure was developed and implemented for the MTA Optical Refractometer. The procedure consists of layering a series of solutions having known refractive indices into both of the MTA Fluids Optical Cells (FOC), and acquiring the imaged profiles for a series of optical configurations. The images are analyzed using the image processing software, and evaluated to produce coefficients that relate the imaged refractive index profile (offset distance) to the known refractive indices through the geometrical configuration of the refractometer. Software was developed to implement this analysis, and to produce calibration coefficients for refractive index predictions based on the MTA optical geometry and imaged profiles.

The optical calibration is valid as long as the fluid cell assembly is not disturbed within the support frame, as happens when the assembly is taken apart to replace a membrane or repair a leak. Disassembly alters the optical geometry of the fluid cells relative to the incident laser, the membrane, and to the other fluid cell. A refractometer calibration is performed simultaneously on both of the two fluid cells (Upper & Lower). The MTA is first assembled complete with membrane and support grids in a leak free configuration within the support frame. The FOC support frame is then securely attached to the optical mount in the MTA instrument, and leveled. Care is taken not to minimize vibrations and disturbances to the assembly during the subsequent calibration activities.

Three fluid layers of known refractive index are carefully introduced into the FOC's (three layers in each fluid cell). The fluid in the lower FOC does not contact the membrane to avoid osmosis and the associated mixing of the fluid layers. The peristaltic pumps are used to deliver about 7 cc fluid volume into each of the layers, in each of the fluid cells. The pumping rate is set very low ($\sim .05$ cc/sec) to minimize fluid turbulence during these filling operations. The fluid tubing is purged between the fluid layers to minimize the mixing between solutions and layers.

Once the calibration solutions are in place, calibration images are acquired for a series of refractometer geometry's. There are the two primary variables in the refractometer geometry: (1) MTA Rotation Angle (Theta) and (2) Projection Distance. Theta defines the laser beam incidence angle relative to the fluid cell, and the projection distance is a measure of the distance the refracted beam travels to the projection screen. Figure 24 shows a schematic of the MTA refractometer, and how these two variables affect the optical geometry.

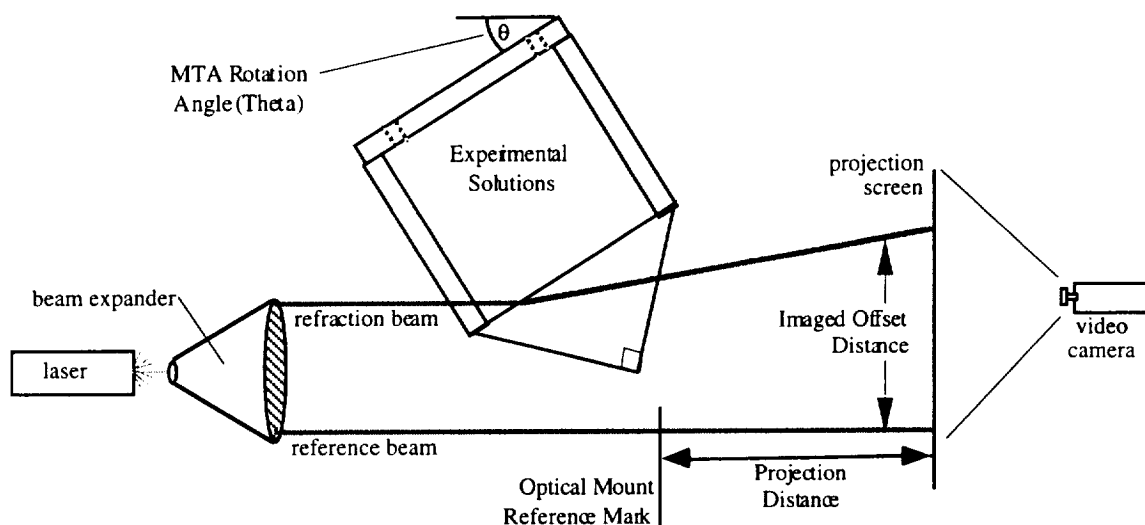


Figure 24 MTA Refractometer Schematic Diagram and Calibration Variables

Calibration data is acquired as a series of refractive index profile images with the MTA geometry varied to cover an operational range of parameters. The rotation angle (θ) is set using the rotary table on the optical platform, and images acquired for a series of projection distances as set on the MTA optical rail. In this way, each of the geometrical variables is iterated, and images obtained for configurations that span the refractometer space. The projection distance is measured from a reference mark on the optical platform, and is only an approximate value. The precise projection distance associated with each rotation angle is determined in the calibration analysis.

The calibration images are acquired from the color video camera using the frame grabber board. The laser operates at 630 nm (red), and the red plane of the color image contains all of the information in the image. The red plane is extracted and converted to an 8 bit grayscale image for further analysis. Each of the calibration images is processed in this way. The rotation angles is varied from 24° to 28° in 1° increments, and projection distance is varied from 5 to 30 cm. Figure 25 shows the series of (extracted red plane) calibration images acquired with the three layer sucrose solutions as the calibration fluids. Each row of images in the figure represents a constant projection distance, and each column a constant rotation angle.

The figure on the left side of each image is the calibration scale, used by the image processing software to determine three image parameters: (1) calibration of the dimensional scale (2 mm between each calibration line), (2) to establish a reference baseline for measurement of the refractive index profile (horizontal line on upper boundary of the calibration figure), and (3) to determine the plane of the membrane (longest vertical line in calibration figure). The dimensional scale is determined by a statistical analysis of the interval distribution between grid lines, and is applied to measurement of the refracted profile on a pixel by pixel basis. Figure 26 shows the output from the image processing software for $\theta = 26^\circ$ and Projection Screen Index = 38 cm.

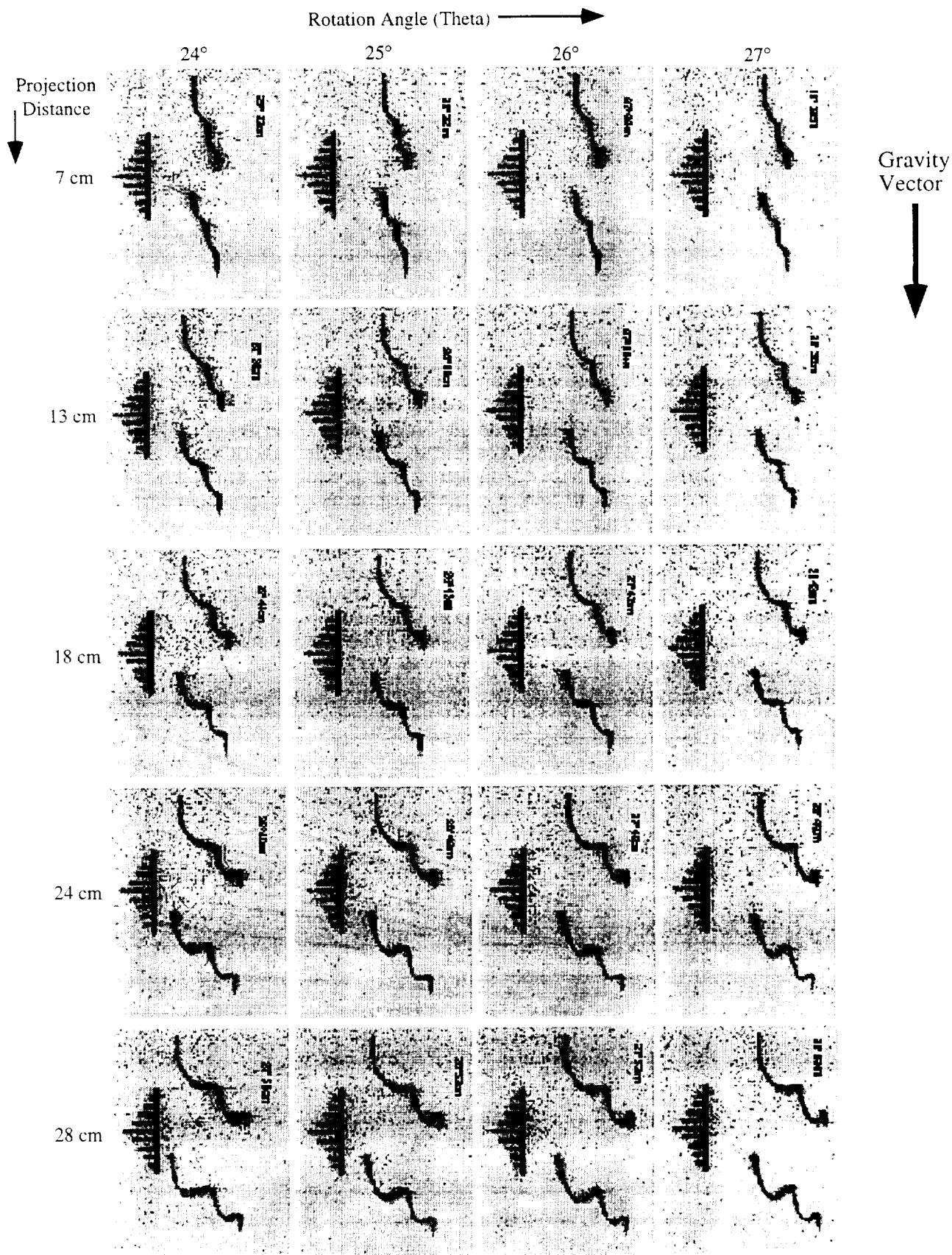


Figure 25 MTA Calibration Image Series for Three Layer Sucrose Solutions. From the bottom, the dissolved sucrose in each layer is 14.0 wt% (16.5° Brix), 9.3 wt% (10.4° Brix), 0.0 wt% (0° Brix)

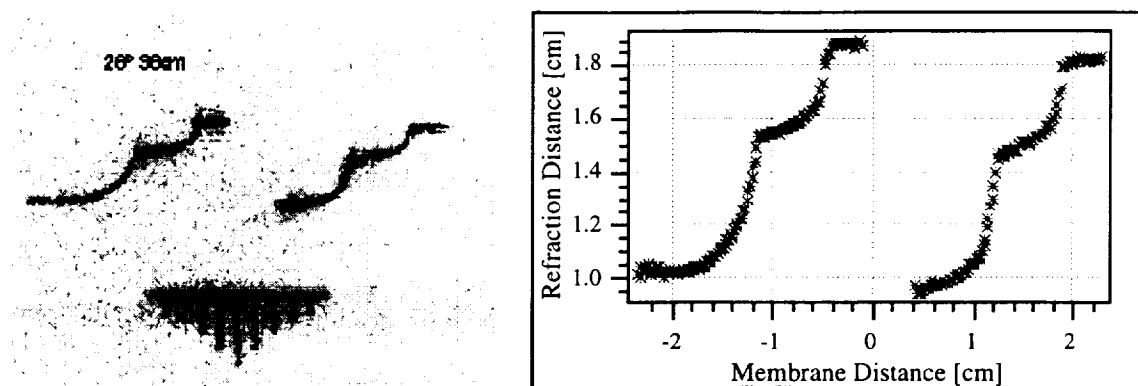


Figure 26 Image Processing Program Example Input Image and Output Data

Each of the images acquired in the calibration procedure is analyzed in this way. This results in a series of graphs that relate the refraction beam imaged offset to: (1) the solution index of refraction, (2) the MTA rotation angle (Theta), and (3) the image projection distance. The image data are tabulated to enable analysis of the calibration geometry, and an analysis performed to characterize the projection distance relationship to the MTA geometry. This analysis results in a point in space that defines the refraction angle (Alpha) and reference beam offset distance from the calibration baseline. The imaged offset data are then ordered as a function of projection distance, rotation angle, and refractive index. The imaged offset dimension associated with each rotation angle and refractive index are then plotted as a function of projection distance to determine the optical center of the instrument. Figure 27 shows a plot of these imaged distances as a function of projection distance for all rotation angles and solution refractive indices tested. The plot shown here is only for the upper FOC, a similar analysis is required to calibrate the lower FOC.

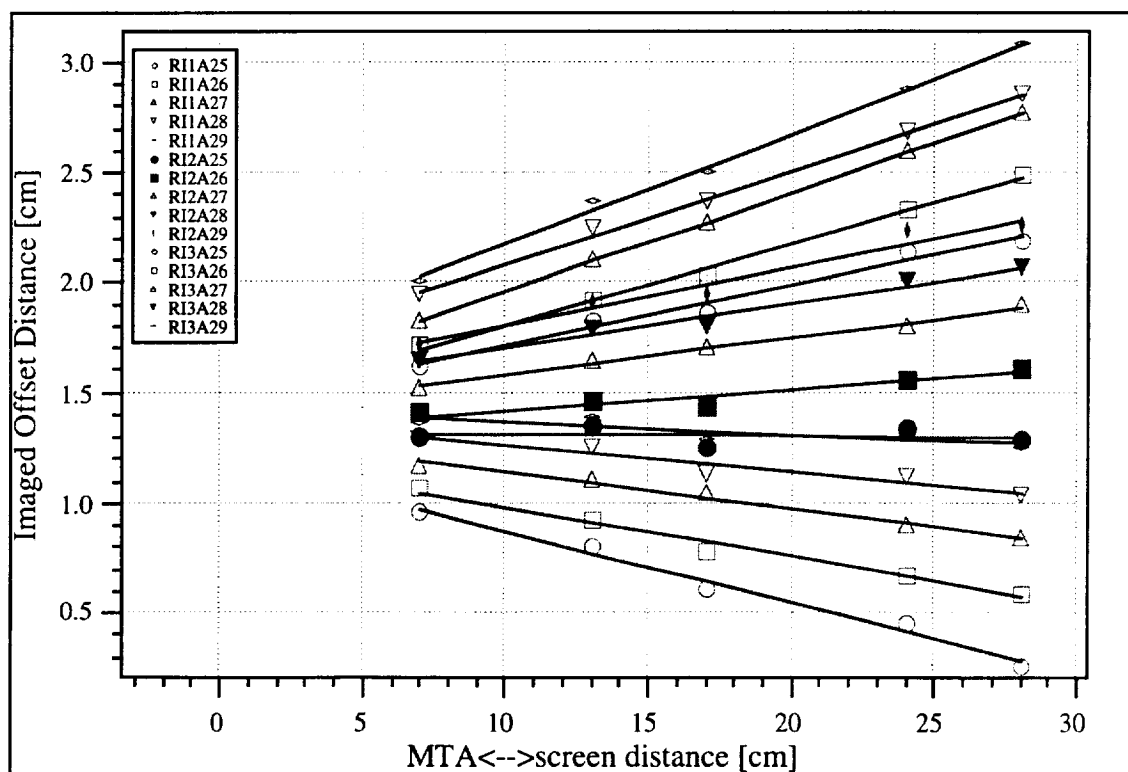


Figure 27 Projection Distance Analysis for all Solution Refractive Indices and Rotation Angles in the Calibration Experiment for the Upper FOC

Linear fits to the data converge to a single point in space. This point represents the optical center of the MTA, and defines the exact projection distance and offset of the reference beam relative to the refraction beam. The calculation of this point in space is key to the refractometer calibration. Knowledge of this point allows precise measurement of the projection screen distance and the offset distance to be defined by the calibration figure baseline plane. These two dimensions are then used to calculate the refraction angle (α), which is directly related to the fluid refractive index.

There are three solution refractive indices associated with each rotation angle θ , all originating from the same point in the FOC prism. An analysis is performed to calculate the intersection of each of the pairs of lines and establish the MTA optical center. Figure 28 shows an example of this analysis, where the linear regression fits to the raw projection distance data are used to compute the intersection points. The three intersection points are then averaged to determine the MTA optical center associated with each rotation angle θ .

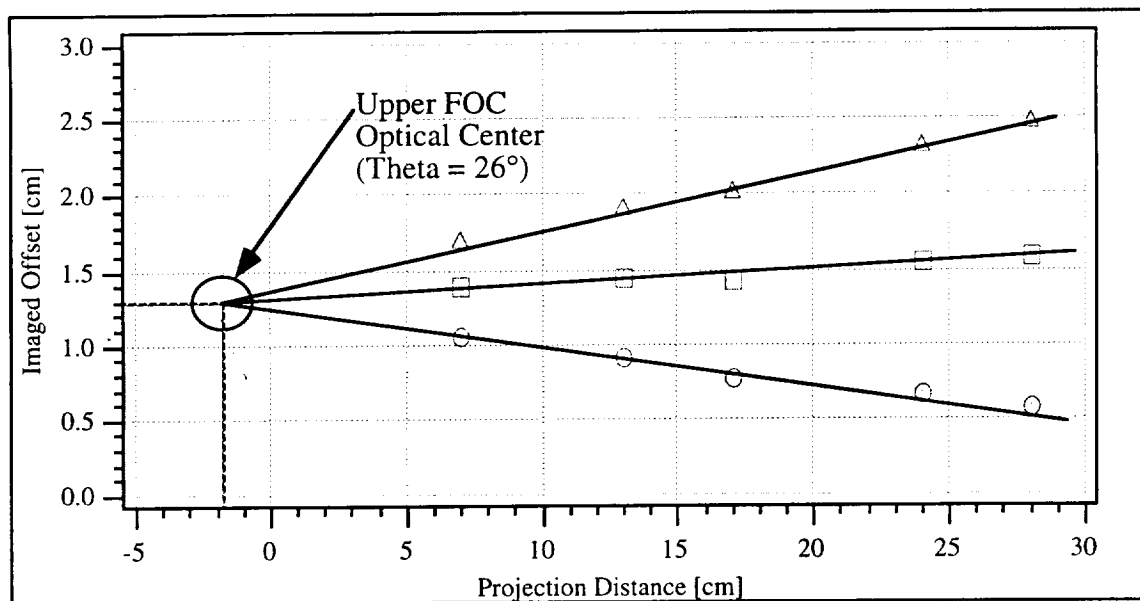


Figure 28 MTA Refractometer Projection Distance Calibration for $\theta = 26^\circ$. Each pair of lines intersect at a point in space. The three intersections are averaged to define the MTA Optical Center for Each Rotation Angle θ .

The projection distance intersection is seen to be a negative number. This is a geometrical artifact that occurs because the MTA reference mark (located at 0 on the x-axis) is located physically in front of the MTA optical center. The calibration distance determined in this analysis is simply an additional distance that is added to the reference Projection Distance as a calibration offset value. The intersection of the reference point on the graph y-axis represents the refraction beam offset distance relative to the reference beam on the laser slit mask. This offset distance is 1.50 cm on the slit mask, and is calculated at values close to this in this analysis. This calibration offset value is subtracted from the imaged distances to enable calculation of the refraction angle α . Figure 29 shows the geometry associated with this calculation, and how the two legs of the right triangle are used with the inverse tangent function to compute the refraction angle.

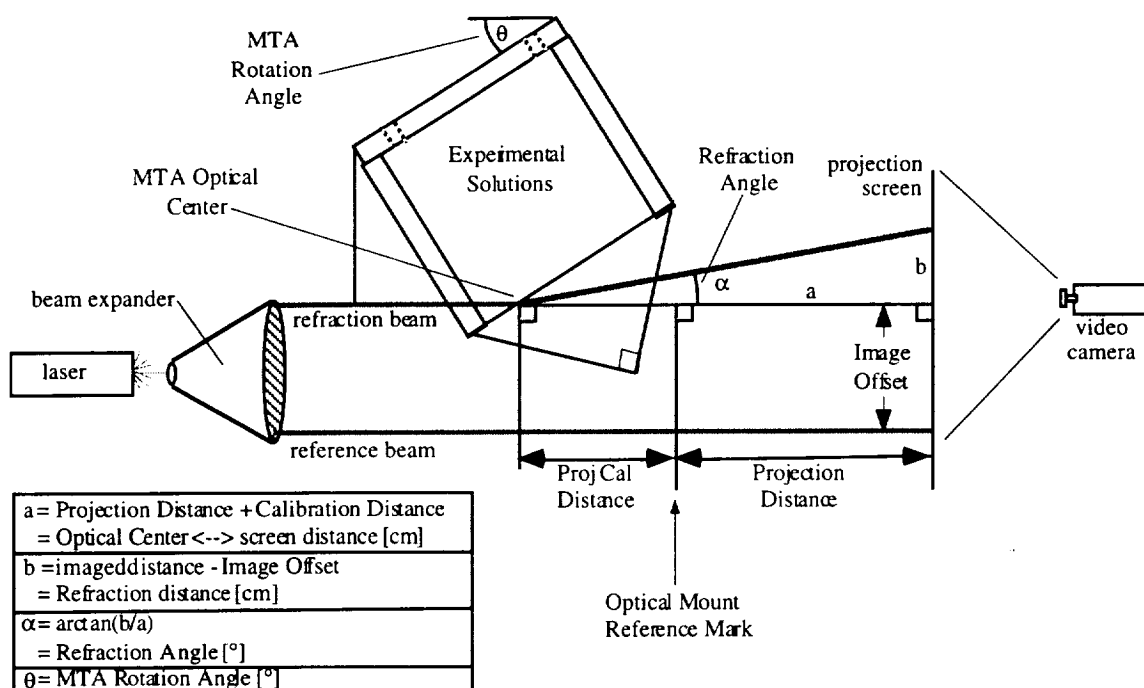


Figure 29 Schematic Diagram Showing Calculation of Refraction Angle (α)

The refraction angle α is directly related to the solution index of refraction. Figure 30 shows the relation between the calculated refraction angle and the solution index of refraction, for each MTA rotation angle (θ). This relation is seen to be linear at a constant θ , as was predicted by the analytical model of the MTA refractometer described in the first MTP Technical Report (May 1996).

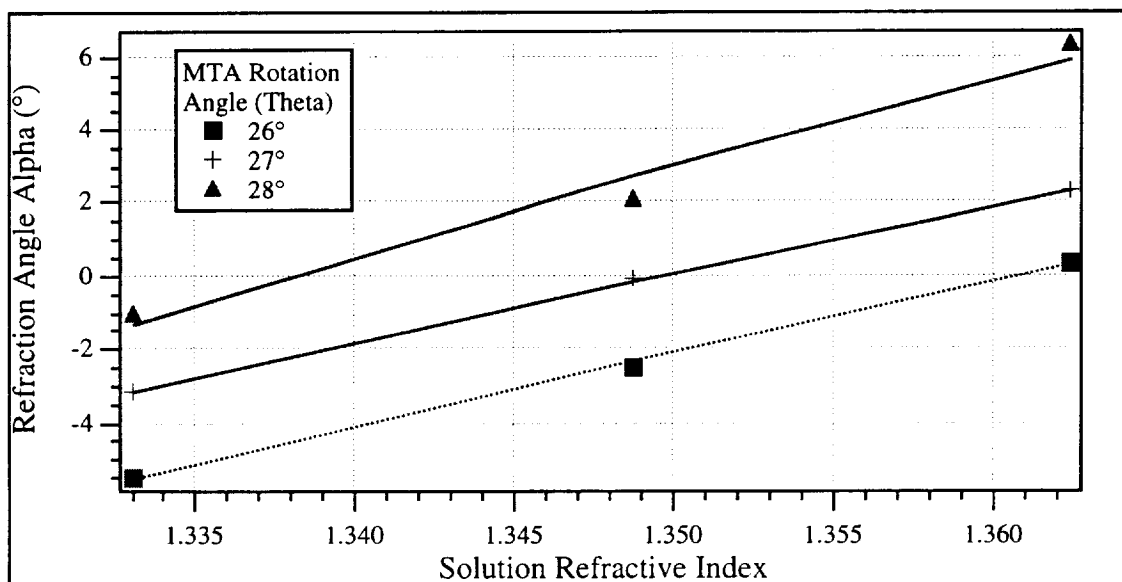


Figure 30 Linear Regression Analysis of Refraction Angle α vs Solution Index of Refraction for Three MTA Rotation Angles (θ)

This calibration procedure characterizes the refractometer performance for multiple MTA rotation angles and projection distances. It was developed to see how the various refractometer geometrical parameters and settings interact in terms of the imaged profiles,

and to optimize the settings. The MTA refractometer operates at a constant rotation angle and projection distance. These geometrical variables can be manipulated to optimize the resolution of the refraction profiles for the various solutions that are used in osmosis experiments.

The Alpha vs index of refraction data can be further analyzed using linear regression fits, and the resulting coefficients plotted in relation the rotation angle (Theta). However, this isn't necessary for operation of the refractometer at a fixed rotation angle. A linear regression fit of the refraction angle (Alpha) as a function of solution refractive index for the appropriate rotation angle results in two final calibration coefficients that can be used to determine the imaged solution refractive index as a function of refraction angle alpha at a constant MTA rotation angle (Theta). The refraction angle (Alpha) is measured in the MTA as one angle in the right triangle formed by the MTA, the projection screen, and the imaged offset distance. Alpha is the inverse tangent of the imaged offset distance divided by the projection distance. The MTA projection distance set on the optical rail, and the MTA rotation angle (Theta) is set on the rotary optical platform. The procedure to reconstruct the solution index of refraction is summarized in Figure 31.

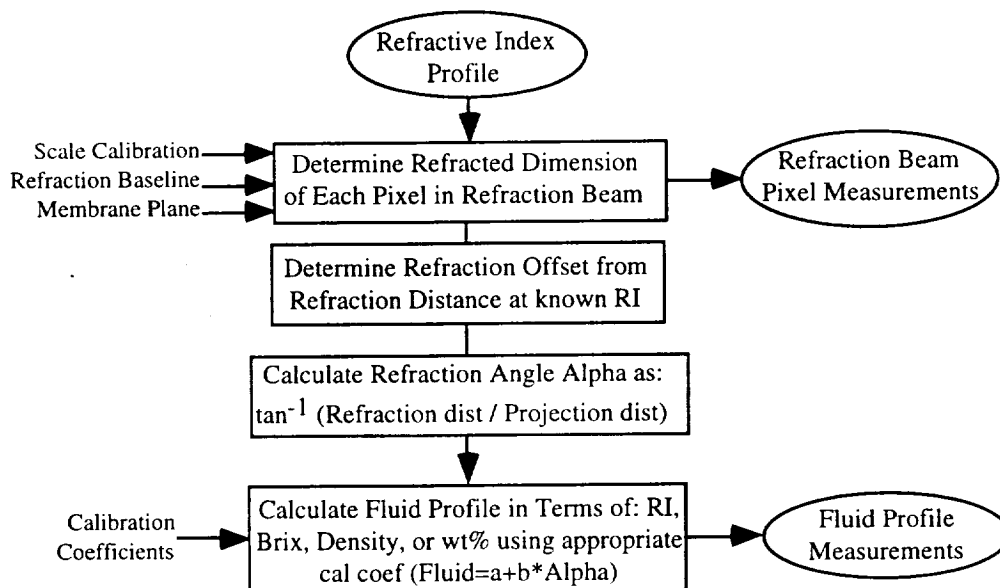


Figure 31 Procedure to Reconstruct Solution Index of Refraction from Imaged MTA Refractometer Profiles.

MTP ANALYTICAL MODEL DEVELOPMENT

A computational model is under development for the MTP experiment. When complete, the model will be used to generate predictions of fluid behavior for either of two MTA convective environments: enhanced or inhibited convection. At present, the model includes only diffusive transport among a series of volume elements defined by the MTA geometry. It will be upgraded to include the bulk flow effects associated with osmotic transport phenomena.

The position of the colligative solution relative to the gravity vector defines the convective environment within the MTA. The two convective modes that the MTA can produce (enhanced or inhibited convection) are each modeled by different algorithm. The enhanced convection orientation (+1g) uses equations that govern the behavior of a stirred tank

reactor to model the fluid profile. In this orientation, gravity driven convection acts to mix the colligative solution in concert with osmosis. The alternate MTA orientation where convective effects are inhibited ($-1g$), produces stably stratified fluid layers in association with the membrane. The developmental kinetics of this fluid structure are described by a differential equation, whose coefficients determine the behavior of the fluids over time. Table 4 lists descriptions of the convective environments and computational algorithms used to model the MTA system. The microgravity fluid convective environment has not yet been characterized or modeled.

Table 4 Gravimetric Orientations of the MTA

Gravity Vector	Gravimetric Orientation	Convective Environment	Fluid Structure	Analytical Model
+1 g	solute on top	enhanced convection	unstably stratified layers	stirred tank reactor
-1 g	solute on bottom	inhibited convection	stably stratified layers	finite difference grid
0 g	n/a	zero convection	stratified layers ?	TBD

The MTA Analytical Model is written in C language, and is compiled prior to use. It contains user defined variables for gravimetric orientation of the solutions, solute and solution properties, fluid cell and volume element geometry, output data timing, and datafile disposition. The model algorithms also include functions that describe specific membrane characteristics, physical properties of the solutions, and hydrostatic and osmotic flow effects.

The MTA geometry is modeled as a one dimensional grid, with each node in the grid defining a fluid volume element. The grid is oriented along the long axis of the MTA fluid cells, and is measured relative to the plane of the membrane (membrane is adjacent to volume element zero). The model assumes that the membrane is rigid within the MTA (*i.e.*, no pillowing occurs), and the fluid cells have a constant cross sectional area along the grid axis that is equal to the surface area of the membrane. The Volumetric Flow Sensors are not included in this model. It is assumed that the volume of solution contained within the sensors is small compared to that of the fluid cells, and the contained volume is physically far enough from the fluid adjacent to membrane so that no fluid effects are present. This assumption simplifies the model to that of a pure, one dimensional, diffusion driven system. Figure 32 shows a schematic diagram of the geometrical aspects of the MTA Analytical Model.

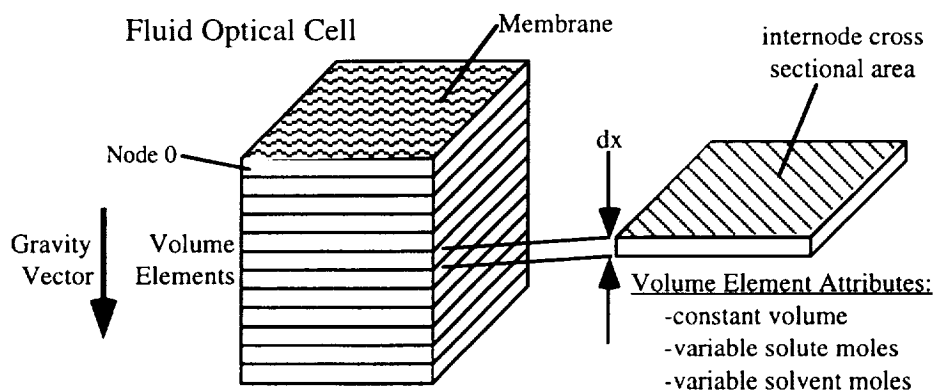


Figure 32 MTA Analytical Model Schematic Diagram in the Inhibited Convection Orientation ($-1g$)

Each of the volume element nodes are separated by the constant cross sectional area of the fluid cell. Diffusive transport among the volume elements occurs over time, with the flux between elements determined by the Diffusion Equation [1], a second order, partial differential equation.

$$\frac{\partial C_a}{\partial t} = D_{ab} \frac{\partial^2 C_a}{\partial t^2} \quad [1]$$

Diffusion Equation Coefficient Identification:

C_a = colligative solute concentration [molar]

D_{ab} = diffusion coefficient for solute in water [cm²/s]

t = time [s]

Equation [1] has been discretized for computational use. The algorithm used to discretize the differential terms is an explicit expression based on a Forward in Time, Central in Space (FTCS) approximation. After this transformation, the equation was solved for the unknown solute concentration at successive intervals in time. The finite difference form of this equation, solved explicitly for predicted solute concentration within a single volume element is shown in Equation [2].

$$C_{x,t+1} = C_{x,t} + \Delta t * D_{ab} \frac{C_{x+1,t} - 2C_{x,t} + C_{x-1,t}}{\Delta x^2} \quad [2]$$

Coefficient Identification:

$C_{x,t+1}$ = solute concentration at next time interval [molar]

$C_{x,t}$ = solute concentration at current time interval [molar]

$C_{x+1,t}$ = current solute concentration in adjacent volume element [molar]

$C_{x-1,t}$ = current solute concentration in other adjacent volume element [molar]

D_{ab} = diffusion coefficient for solute in water [cm²/s]

Δt = time interval [s]

Δx = volume element linear dimension [cm]

This computation is performed over all of the volume elements in the grid, each iteration advancing the nodal concentration by one time step (Δt). The magnitude of the time step is limited by the convergence criteria of the finite difference scheme. The convergence stability criteria that applies to this computation series is shown in Equation [3], solved for the maximum allowable time step.

$$\Delta t \leq \frac{\Delta x^2}{2 D_{ab}} \quad \begin{array}{ll} D_{ab} [=] & \text{cm}^2/\text{s} \\ x & [=] \text{cm} \\ t & [=] \text{s} \end{array} \quad [3]$$

The dimensional units for each of the terms of Equation [3] are shown to the right of the equation. The value of the time step must be less than or equal to the quotient shown to insure a converging (stable) solution. Values greater than this result in an unstable computational series, nodal concentrations less than zero, or calculations that attempt to divide by zero. The MTA analytical model incorporates a stability check calculation to insure convergence. The value input for grid spacing (Δx) is used to calculate the maximum allowable time step for stable solution via the relation shown in Equation [3],

and compared to the input time step. If the input time step is too large, the MTA model halts execution and outputs an error message that lists the maximum allowable time step for the defined grid spacing.

A grid spacing of 175 μm per volume element has been selected for general use in the MTP model, based on the nominal pixel resolution obtained in the MTA refractometer images. At this grid spacing, approximately 200 volume elements fit within the MTA fluid cell geometry. Using this node spacing (Δx), the upper limit on the time step is about 1.5 seconds to insure a stable solution for a diffusion coefficient of $1 \times 10^{-4} \text{ cm}^2/\text{s}$. This time step is small enough that substantial periods of computation time are required to compute the transient fluid profiles ($\sim 60,000$ iterations for 24 hours of model elapsed time). The grid spacing can be increased to increase the allowable time step, with an associated decrease in spatial resolution. The increased grid spacing is useful for preliminary analyses where the loss of resolution from fewer volume elements is not critical.

Preliminary analyses were performed to verify that the functionality of this finite difference diffusion algorithm. The boundary conditions used for the verification were a constant zero solute concentration at the membrane, and a constant solute concentration at the outside edge of the fluid cell. Figure 33 shows the results of one of these analyses, with the solution concentration shown as a function of time for several nodes within the fluid cell, spaced at the distances shown in the legend. The solute modeled in this run was sucrose (Mol Wt: 342.5), with an initial concentration of 5 wt% ($\sim 150 \text{ mM}$), and a diffusion coefficient of $1 \times 10^{-4} \text{ cm}^2/\text{s}$.

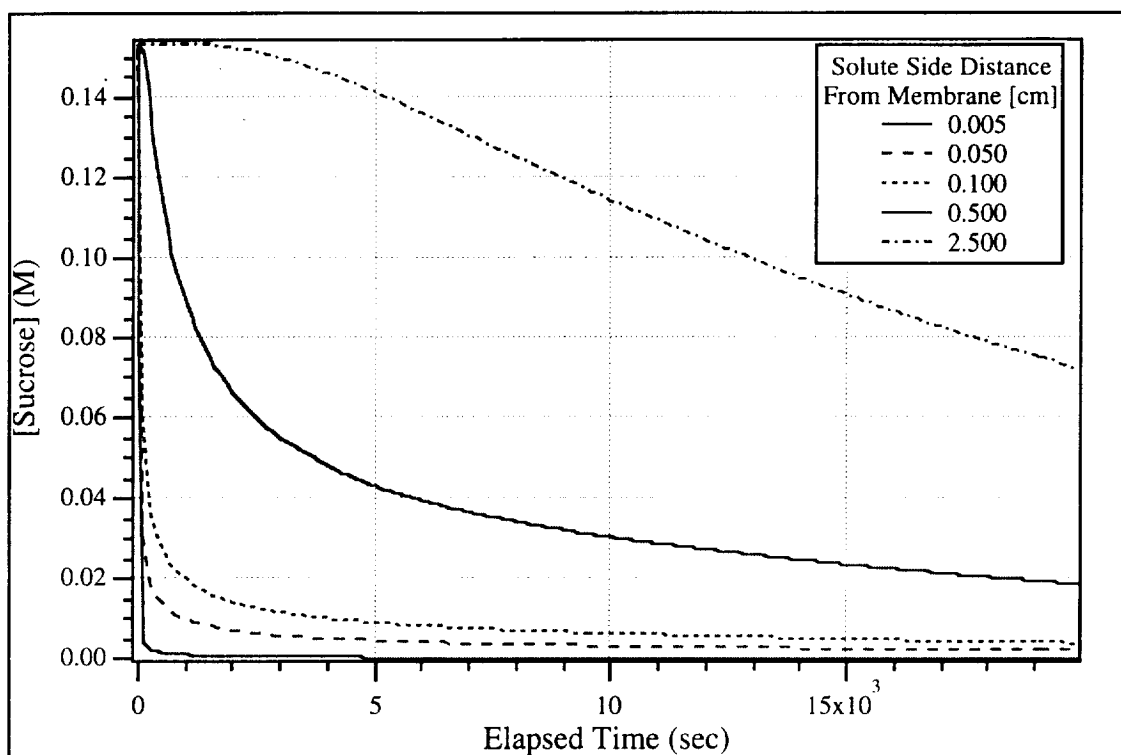


Figure 33 MTA Analytical Model, Constant Boundary Conditions, Pure Diffusion Predictions for $D_{ab} = 1 \times 10^{-4} \text{ cm}^2/\text{s}$

The model will be upgraded to include more realistic boundary conditions and bulk flow effects. Osmotic and hydrostatic flow characteristics that are associated with specific membrane types will also be included. As described in previous sections of this report, the

Volumetric Flow Sensors (VFS) have provided data for trans-membrane flow rates as a function of hydrostatic pressure (ΔP) and osmotic chemical potential ($\Delta \mu$). These flow characteristics will be fit to polynomial equations using data obtained from the MTA experiments. The polynomials will then be used as empirical relations to define the membrane boundary condition (grid element 0) for each computational time interval. The driving force for osmosis is then defined by the colligative solute concentration in the volume element adjacent to the membrane.

DC-9 MICROGRAVITY EXPERIMENT DEVELOPMENT

Two experiments are planned for the MTP DC-9 microgravity flights: (1) testing the Fluid Manipulation System (FMS) to transfer fluids within various test cell geometry's, and (2) Refractometer Verification Experiment (RVE) for the observation of fluid refractive index under microgravity conditions. The two experiments are run separately, and share equipment within the MTP experiment rack. The microgravity flights are currently scheduled for the week of 16 December 1996. A MTP Safety and Engineering Document was generated and submitted to NASA in preparation for the flights. This document describes the experiment in detail and lists several engineering analyses required for flight.

Fluid Manipulation System (FMS) Experiment

Two candidate MTP Fluid Optical Cell (FOC) geometry's have been developed for this experiment: (1) Quarter Circle cell and (2) Triangular cell. These test cells each have a different internal geometry, and will be tested to assess the completeness of filling and draining, and the propensity to trap air bubbles or leave fluid behind during fluid manipulation procedures in microgravity. The cells are sized to allow complete filling/draining within the ~20 seconds of microgravity afforded by each parabolic dive. During the course of performing these experiments, it is anticipated that incomplete filling or draining will occur in some instances. In this event, a small interval of time (<30 seconds) is required to reset the fluid cells to an initial condition in preparation for the next dive.

The filling/draining operations will be conducted in each of the candidate fluid cells for a series of fluid pumping rates and filling schemes, one scenario per parabolic dive. For each scenario, one dive will be used to fill the fluid cell, and the subsequent dive used to assess the draining operation under the same experimental conditions. Thus, a minimum of two parabolic dives is required for each fluid manipulation condition. Repeat experiments will be conducted at successful pumping rates as flight conditions allow.

Colored, deionized water is used in all FMS experiments to visualize the fluid flow patterns. The two MTA computer controlled peristaltic pumps are used to automatically manipulate the fluids during microgravity, with each experiment initiated by a single mouse click at the onset of a parabolic dive. A Video Cassette Recorder (VCR) will acquire image data showing the completeness of filling/draining. The video system includes a character generator that is interfaced to the computer to allow real time display of elapsed time and g-level data directly over the fluid cell images during filling operations.

Refractometer Verification Experiment (RVE)

The second experiment for the MTP microgravity flights involves verification of optical refractometer performance. These tests involve the visualization of fluid refractive index as a function of gravity level for a variety of fluids using a small (hand held) refractometer that is secured to the experiment rack. The fluids used in these experiments are all non-hazardous aqueous solutions. Prior to a parabolic dive, a small quantity (~3 drops) of the test solution is placed onto the refractometer sensing element using a liquid dropper (in 1-g). The fluid is contained on the refractometer sensing element by a plastic cover, so no

fluid can float free during microgravity. The experiment consists of visualizing the solution refractive index during the parabolic dive, with the image of the refractometer optics acquired using the video system. The Refractometer Verification Experiment will be repeated using various experimental fluids as time and flight conditions allow.

DC-9 Experiment Hardware Description

The hardware used in these experiments consists of electrical and mechanical instruments that are mounted within an equipment rack. The rack was obtained from NASA/MSFC, and has parabolic dive flight heritage. It was previously used for the Phase Partition Experiment (PPE) instrument package flown on the KC-135 in May 1995. The total mass of the MTP equipment is less than that of the PPE that has already flown using this rack. The equipment rack measures 27" x 27" x 44", and contains all of the MTP equipment within the three internal shelves. The equipment consists of a computerized Fluid Manipulation System that includes various fluid test cells, peristaltic pumps, electrical interface circuits, valves, power supplies, refractometer, video camera, VCR, computer, monitor, keyboard, and mouse. Figure 34 shows a schematic of the equipment and the relevant interconnections.

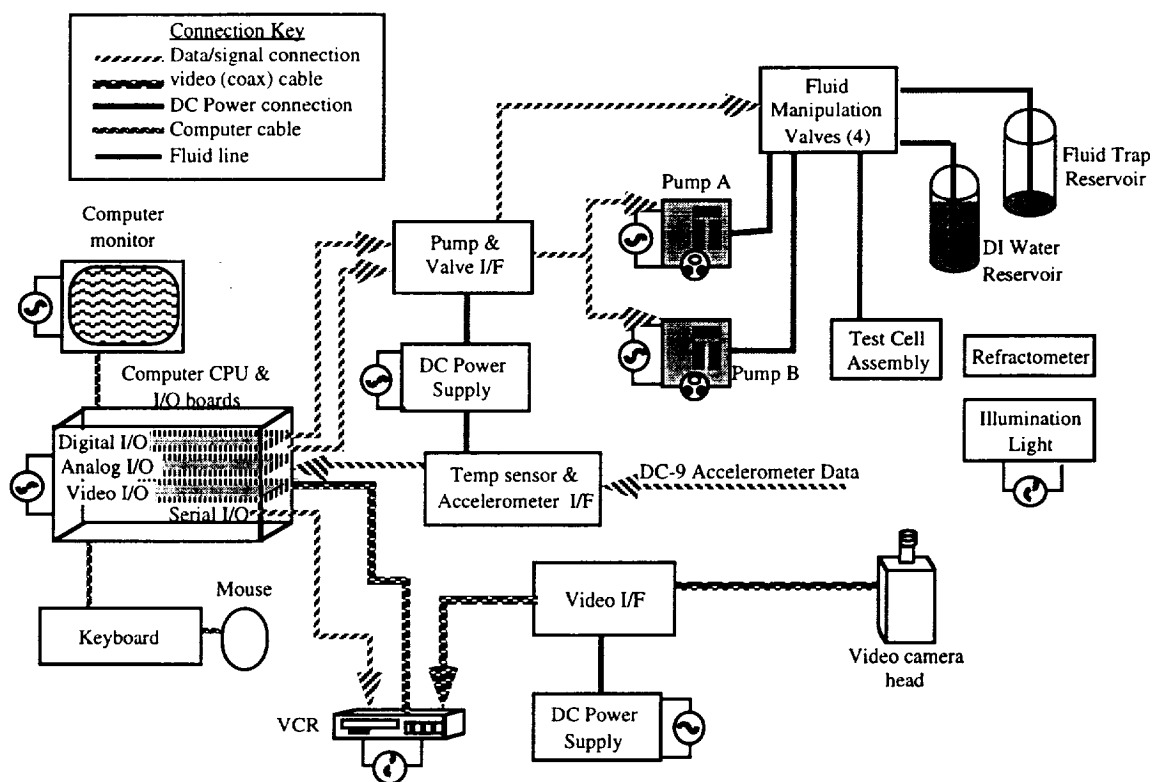


Figure 34 MTP DC-9 Microgravity Flight Experiment Equipment and Interconnections

The two experiments planned for the DC-9 flights share various components within the MTP equipment rack. The computer acquires data from the DC-9 accelerometers and a temperature sensor. The computer monitor displays both the video images through an internal frame grabber I/O board, and the acquired accelerometer and temperature data. In addition, the computer is interfaced to a VCR character generator that displays real time data directly on the video images. The VCR records the data and experiment images during the parabolic dives, to be used for post-flight data analysis and review of the experiments. Figure 35 shows the mechanical equipment layout within the MTP equipment rack. All dimensions are in inches.

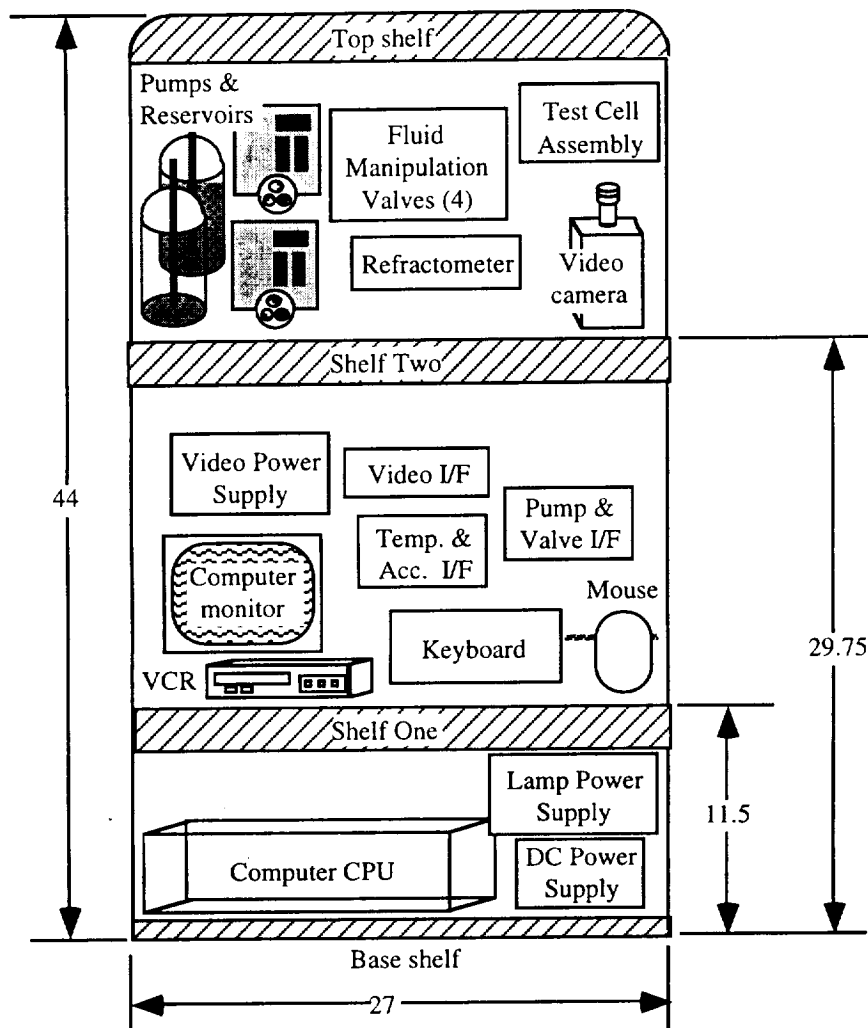


Figure 35 Mechanical Layout of MTP Equipment for the DC-9 Microgravity Flight Experiment

In the FMS Experiment, peristaltic pumps are used to fill and drain candidate fluid cells while the video system images and records the operations. The fluid cell geometry's will be assessed for completeness of filling/draining, and the propensity to trap bubbles in microgravity. These tests will be run for a variety of pumping rates and filling scenarios. The fluid to be pumped is deionized water, and is contained within a microgravity tolerant fluid reservoir that is securely fastened to the equipment rack. The fluid reservoirs are designed to captivate the fluid within a defined volume during microgravity, and insure the peristaltic pumps are primed during the microgravity fluid transfer operations.

The FMS Experiment plumbing diagram is shown in Figure 36. The two test cells that will be used (quarter circle and triangular) are interchangeable within the FMS; both will be tested in the course of the microgravity flights. The pumps are peristaltic, and are under control of the computer. The fluid reservoir is a modified 500 ml Pyrex media bottle that is sealed with an internal bladder to maintain pump prime during periods of microgravity. The open circles in the Flow System Schematic indicate connections to a second fluid reservoir that has been modified to trap any fluids that enter. This reservoir provides the fluid loop interface to the cabin atmosphere. These ports interface to this reservoir, serve to

contain any fluids that may try to exit the apparatus, and are the air inlets for fluid cell draining operations.

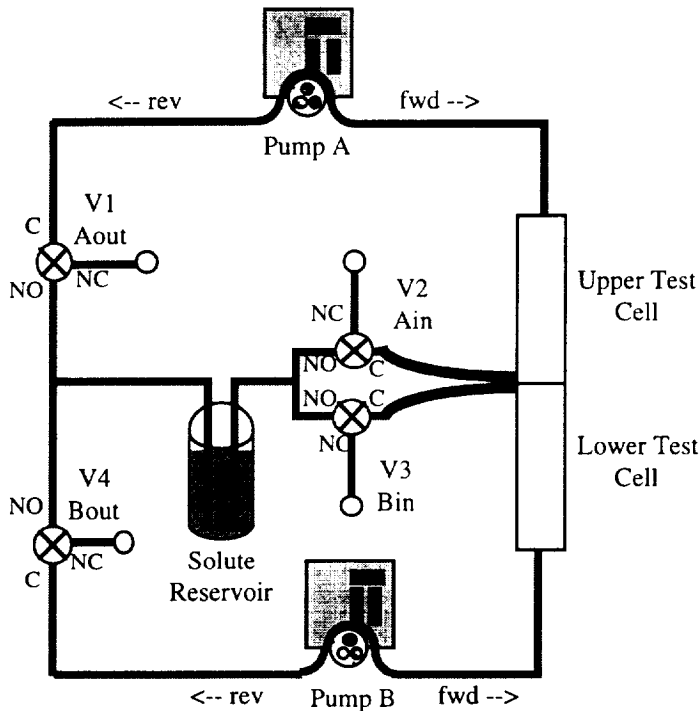


Figure 36 FMS Experiment Flow System Schematic

The computer is the experiment control center, initiating programmed pump sequences, coordinating control actions, and providing real time display of acquired data. Software modules have been written to control the experiments and acquire data from the DC-9 accelerometers during parabolic dives. These data acquisition functions are interfaced through a video character generator to overlay real time data on the video images of the test in progress. Figure 37 shows the user interface for the DC-9 experiment control panel. The video image is displayed within a separate window on the computer monitor, a separate video monitor is not required to view the video images.

The fluid pumping operations are under control of the computer. The script interpreter described in the Fluid Manipulation System section of this report has been modified to orchestrate the pump and valve operations for filling and draining the test cells in this DC-9 experiment. The scripts have been tailored to the specifics of filling and draining the test cells through a variety of orientations, and for resetting the fluid to known states in 1g. The initiation of an experiment is accomplished through a single mouse click prior to the onset of a parabolic dive. The pumping speed and fluid manipulation script are selected using the controls shown at the top of the panel, and initiated by actuating the "GO" button with a mouse click. The fluid manipulation operation then proceeds and terminates autonomously during the parabolic dive. Additionally, the valves can be manually commanded to actuate through a graphical user interface showing a schematic representation of the flow diagram.

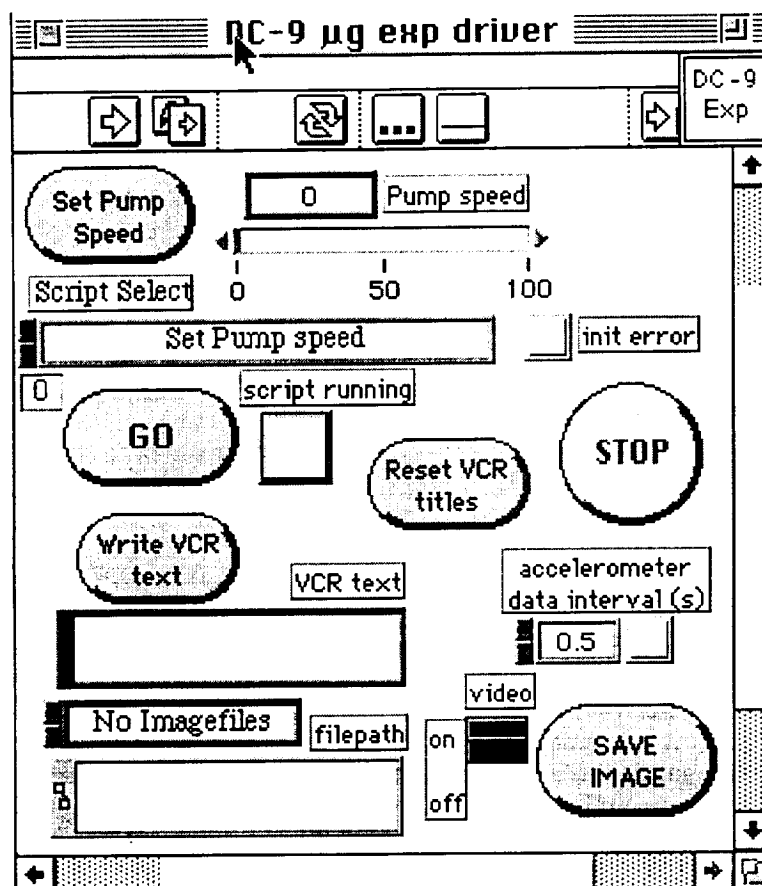


Figure 37 DC-9 Flight Experiment Software User Interface and Control Panel

Several analyses were performed to document the MTP DC-9 Flight Experiment characteristics, and verify that the mechanical design of the support structure is robust enough to withstand the rigors of the parabolic dives. These analyses included structural, mechanical, electrical, and hazard identification.

An Excel spreadsheet was generated to perform a structural analysis on each piece of equipment mounted within the rack. The moment arm for each was calculated as the product of the equipment Mass (lb.) and the lever Arm (in) measured from the base of the rack. Each equipment item was weighed in the laboratory using a triple beam balance (20 kg capacity). The equipment rack weight and moment maximum limits were supplied by NASA/MSFC for comparison with the calculated values. In all cases the weight and moment limits for the rack were not exceeded.

A separate analysis was performed to determine the stress and strain imposed on fastener hardware for the MTP experiment equipment under a 9 g load. The material stress and strain limits were taken from the Metals Handbook (10th Edition) for (Grade II) steel threaded rod and nuts, Aluminum tiedown straps (Al-2024-T4), and High Strength Aluminum rack structures (Al-6061-T6). These calculations were performed for a 9g acceleration, also in an Excel spreadsheet. The calculation results were then compared to the material stress and strain limits. In every case, the load on the fasteners under a 9g load was less than the reference material stress and strain limits.

An estimate of the MTP experiment power requirements was prepared, using both nominal and maximal power utilization. The electrical load estimates were calculated for all the

MTP equipment that is connected the 115 VAC - 60 Hz power supplied by the DC-9 aircraft. The maximum electrical current draw was calculated at 10.3 Amps, corresponding to a maximum power utilization of just over 1 kilowatt. The nominal operating current for the MTP experiment is about 7.8 Amps.

A preliminary hazard analysis was performed to determine areas of potential accidents, and to formulate control mechanisms to minimize the advent of a potential mishap. The hazards associated with collision, contamination, corrosion, electrical, environmental/weather, explosion, fire, loss of atmosphere, mechanical, pathological, psychological, radiation, and temperature extremes were explored and identified. The results of the analysis were documented and the associated risk elements categorized in terms of a risk assessment matrix. This matrix assigns risk codes to each hazard according to the Risk Assessment Code Matrix (MIL-STD-882), encompassing values from 1 (extreme risk) to 20 (negligible risk). The worst risk that was found using this analysis was determined to be an improbable possibility of a critical failure (Risk Code: 15). This was determined for a material defect in the mechanical fasteners used to secure the equipment in the rack.

MICROSENSOR ARRAY DEVELOPMENT

Stanford Research Institute (SRI International) is under contract to fabricate prototype versions of the microsensor arrays that are planned for inclusion in the second generation Membrane Transport experiment (MTA II). This activity is funded by Lockheed Martin Astronautics-Internal Research and Development (LMA-IRAD). The objective of this effort is to develop instrumentation to measure electrolyte concentrations within the developing fluid boundary layer in the MTA. This sensing capability is prerequisite to the MTA II experiment.

The prototype microsensor array development is being performed for several reasons. The primary purpose of the prototypes is to understand the manufacturing process for the arrays. No arrays of this type have ever been developed, and it was anticipated that some problems would be encountered. The microsensor array is being developed in several phases. The first phase is fabrication of prototypes to determine problem areas and develop designs for more advanced versions. The prototypes will also be used to verify the interface electronics for data acquisition, and provide experimental data for proof of the array concept. The prototypes will be evaluated for functionality, and design modifications generated for fabrication of the MTA II arrays, planned for 1997.

The microsensor array design includes a series of sensing elements to measure profiles in anion, cation, electrical conductivity, and temperature. Each sensing element is about 50 μm square, and the elements are spaced at intervals ranging from 50 μm to 5,000 μm . The prototype arrays contain 4 elements of each of the sensors listed. The Ion Sensing Electrodes (ISE) are fabricated using ionophore material that is broadly sensitive to both monovalent and divalent, anions or cations. The ionophore material is deposited in micromachined wells on a ceramic substrate, with electrical contact made using vapor deposited platinum traces. The conductivity and temperature sensors are simply platinum traces laid down on the ceramic in the appropriate geometry. These traces consist of either insulated serpentine patterns (temperature sensor), or small parallel traces that are in direct electrical contact with the solution (conductivity cells). The platinum traces lead to the edge of the microsensor substrate, and terminate at silver pads to which small wires are bonded for electrical access to the sensors. A polymeric insulation material is used to coat the platinum traces to provide insulation from the experimental solutions.

SRI reports that the prototype arrays have been fabricated. Tests on single array elements show the sensors to meet the functional specifications. However, there were some minor

technical problems encountered when laying down arrays of sensors and sealing the insulation material to the ionophore wells on the ISE's. It seems that the insulation material used does not adhere well to the ionophore, and that some leaking was detected. A fluid leak at this point in the ISE causes the sensor to malfunction. Additional problems were encountered in attaching wires to the numerous contact pads for transmission of the sensor signals. Wire bonding techniques have been developed to enable high density connections of this type, but the preliminary technique that was used damaged the original connection pads. Once the pads were damaged, a new layer of silver had to be deposited to form a new connection pad for further wire bonding.

The delivery schedule for the prototype microsensor arrays has slipped to the end of November 1996 because of these problems. The problems are of the type that was expected, and can be solvable through evaluation of the fabrication process and testing and identification of alternate materials. Further array definition and development activity is planned for CY97 under LMA-IRAD funding. The schedule slip does not affect the first generation (MTA I) experiment development.

MICROSENSOR ARRAY INTERFACE ELECTRONICS DEVELOPMENT

The sensor elements within the Microsensor Array each require specialized interface electronics for data acquisition. The electronic circuits include extremely high impedance voltage amplifiers to match the high impedance of the ISE electrochemical cells. The small size of the ISE's further increases the impedance over devices of this type that are physically larger. The conductivity sensor interface requires a high frequency oscillator signal that is transmitted to one of the conductivity cell electrodes. The magnitude of the signal received on the other electrode in the cell is then a measure of the solution electrical conductivity. The signal must be amplified, rectified, and integrated to produce a high level signal suitable for the analog to digital converter and computer data acquisition. A stable current source is required for the temperature sensors, with the voltage drop across each array element then a measure of the element temperature. Specialized cabling is also required to interconnect the sensor arrays, interface electronics, and the data acquisition computer. Circuits for each of these applications have been developed, and are currently being fabricated on a breadboard card module. The module is part of a card cage that will house the microsensor array interface electronics. This activity has been occurring at a low level over the course of the MTP study, as time allows. The microsensor array interface electronics activity is funded as LMA Capital Equipment activity.

